iScience

CellPress
OPEN ACCESS

Article

Maf1 controls retinal neuron number by both RNA Pol III- and Pol II-dependent mechanisms

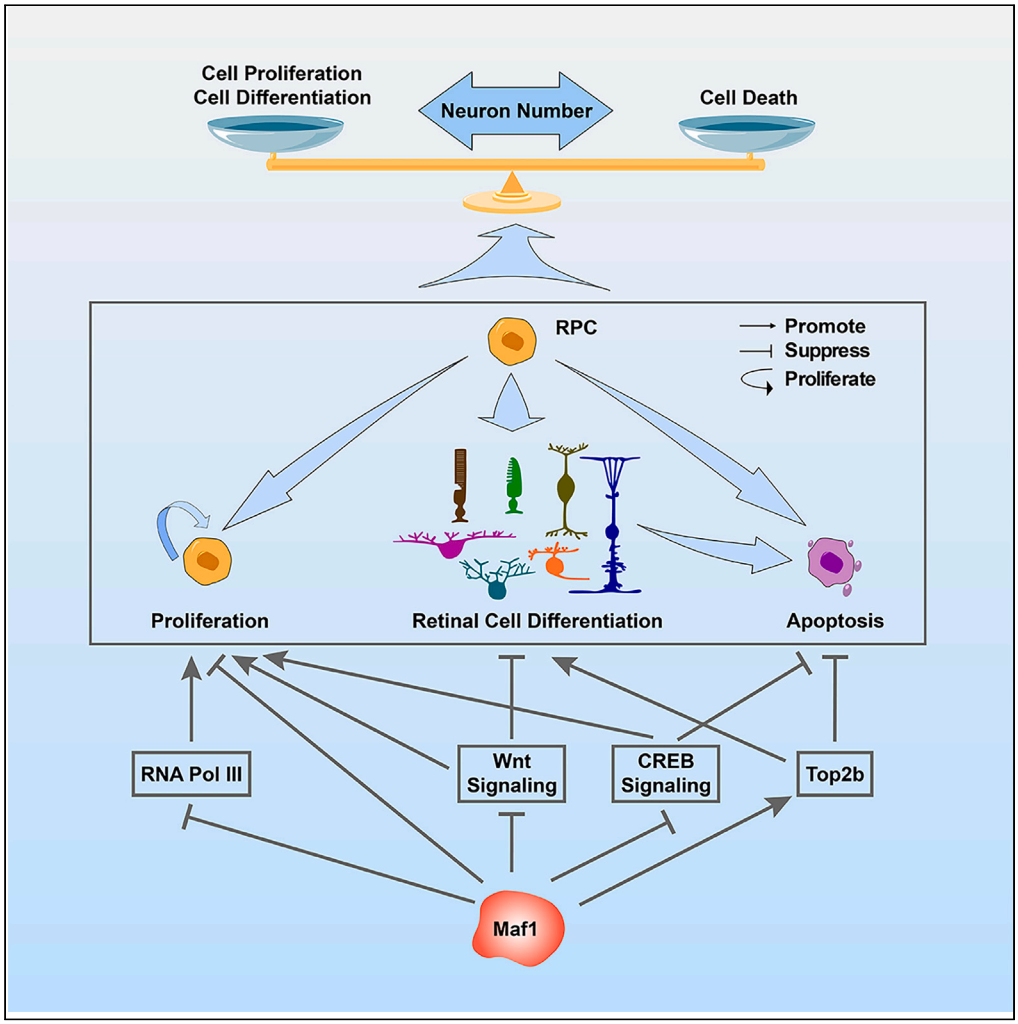

Yifei Li, Dongchang Xiao, Haiqiao Chen, X.F. Steven Zheng, Mengqing Xiang

xiangmq3@mail.sysu.edu.cn

Highlights

Maf1 inactivation results in retinal dysfunction and retinal neuron loss

Maf1 regulates the differentiation of all retinal neuron types

Maf1 negatively regulates retinal progenitor cell (RPC) proliferation

Maf1 binds widely to the genome to regulate the expression of Pol II-transcribed genes

Li et al., iScience *26*, 108544
December 15, 2023
https://doi.org/10.1016/j.isci.2023.108544

iScience

CellPress
OPEN ACCESS

Article

Maf1 controls retinal neuron number by both RNA Pol III- and Pol II-dependent mechanisms

Yifei Li,[1] Dongchang Xiao,[1] Haiqiao Chen,[1] X.F. Steven Zheng,[2] and Mengqing Xiang[1,3,4,*]

SUMMARY

The generation of appropriate numbers and types of neurons is a prerequisite for assembling functional neural circuits. However, the molecular basis regulating retinal neuron number remains poorly understood. Here, we report that inactivation of the RNA polymerase (Pol) III inhibitor gene *Maf1* in mice results in decreased retinal thickness and neuron number that cause attenuated electroretinogram (ERG) responses. Its absence causes aberrant differentiation of all retinal neuron types primarily by an RNA Pol II-dependent mechanism while promoting retinal progenitor cell proliferation via both Pol III- and Pol II-dependent mechanisms. Chromatin profiling and transcription assay reveal that Maf1 binds widely to the genome to regulate the expression of a large set of Pol II-transcribed genes involved in retinal cell proliferation, differentiation, and/or survival. Together, our data suggest that Maf1 may control retinal neuron number by a balanced regulation of cell proliferation, differentiation, and death via both Pol III-dependent and Pol II-dependent mechanisms.

INTRODUCTION

The generation of correct numbers and types of neurons in neural tissues during development is a prerequisite for assembling functional neural networks.[1] The mammalian retina is a multilayered sensorineural epithelium consisting of one glial cell type (Müller cells) and six neuronal cell types: rod and cone cells as photoreceptors, bipolar, amacrine, and horizontal cells as interneurons, and retinal ganglion cells (RGCs) as output neurons. It is thought that these cell types only in appropriate numbers and ratios would be able to organize into optimally functional retinal circuits to detect and transmit light signals to the visual targets in the brain. For instance, there are approximately 6.5 million cells in the mouse retina with a rough rod-to-cone ratio of 35:1 and rod-to-RGC ratio of 140:1 [2,3], and the total number of cells and proportion of each cell type vary little in a given mouse strain.[2–4] It is well known that loss of retinal cell types and change in cell type ratios lead to retinal impairment and diseases such as rod-cone dystrophy,[5,6] enhanced S-cone syndrome,[7,8] glaucoma,[9,10] etc. During retinogenesis, the various retinal cell types are generated from multipotent progenitors in an overlapping temporal order and in stereotyped ratios.[11,12] The bulk of RGCs, cones, horizontal cells, and amacrine cells are born between E11 and P2 while most of the rod, bipolar and Müller cells are produced postnatally before P11.[12,13] In the past, regulatory gene networks underlying the specification and differentiation of different retinal cell types have been studied extensively.[14–17] However, it remains poorly understood as to the molecular basis governing the generation of appropriate number of cells in the retina.

There are three types of RNA polymerases in eukaryotes: RNA polymerase I (RNA Pol I), RNA polymerase II (RNA Pol II), and RNA polymerase III (RNA Pol III), each of which performs different functions. RNA Pol I transcribes all ribosomal RNA (rRNA) except 5S rRNA genes. RNA Pol II transcribes genes of mRNA, miRNA, lncRNA, snRNA, and snoRNA. RNA Pol III is responsible for the synthesis of precursors of transfer RNA (tRNA), 5S rRNA, and other small RNAs, which in turn participate in a variety of functions through post-transcriptional regulation.[18] It has been demonstrated that Maf1 acts as a major repressor of RNA Pol III to regulate lipid metabolism,[19–21] cell proliferation,[20,22–25] tumorigenesis,[20,22–25] lifespan,[26,27] and other biological processes[25,28,29] by inhibiting RNA Pol III-dependent transcription. In addition, evidence has been accumulating to show that Maf1 can also function to regulate RNA Pol II-dependent transcription of select genes. For instance, it occupies the promoters of *TBP* and *EGR1* genes to inhibit their transcription in human glioblastoma cell lines.[30] In mouse hepatocytes, Maf1 inhibits lipogenesis by binding to the promoter of the fatty acid synthase gene *Fasn* to repress its expression.[20] Our recent study has shown that in murine peri-infarct cortex, Maf1 similarly occupies the promoters of and inhibits the expression of CREB-associated genes that promote neural plasticity and repair.[31] Although Maf1 is well known for its transcriptional repressor activity, there is one known case where it acts as a transcriptional activator. In hepatocellular carcinoma cells and hippocampal neuron cells, it directly activates the expression of *PTEN*,[22,32]

[1]State Key Laboratory of Ophthalmology, Zhongshan Ophthalmic Center, Sun Yat-sen University, Guangdong Provincial Key Laboratory of Ophthalmology and Visual Science, Guangzhou 510060, China
[2]Rutgers Cancer Institute of New Jersey, 195 Little Albany Street, New Brunswick, NJ 08903, USA
[3]Guangdong Provincial Key Laboratory of Brain Function and Disease, Zhongshan School of Medicine, Sun Yat-sen University, Guangzhou 510080, China
[4]Lead contact
*Correspondence: xiangmq3@mail.sysu.edu.cn
https://doi.org/10.1016/j.isci.2023.108544

a major tumor suppressor gene and an inhibitor of mTOR signaling, suggesting that Maf1 may be able to function as both transcriptional repressor and activator depending on the promoter contexts and signal inputs.

Emerging evidence has implicated an important role for Maf1 in the regulation of tissue development. It promotes mesoderm induction from mouse embryonic stem cells (ESCs) as well as adipocyte differentiation from the mesodermal lineage.[33] By contrast, its knockdown in ESCs and preadipocytes suppresses adipogenesis.[33] Transgenic overexpression of Maf1 in mesenchyme also facilitates osteoblast differentiation which leads to increased bone mass while its knockdown in stromal cells results in decreased osteoblastogenesis.[34] Surprisingly, reducing RNA Pol III-dependent transcription inhibits osteoblast differentiation although it promotes adipogenesis as expected.[34] Moreover, Maf1 overexpression and direct perturbation of RNA Pol III-dependent transcription result in quite different changes in global gene expression profiles during the differentiation process,[34] indicating that Maf1 may control osteoblast differentiation via a mechanism independent of RNA Pol III.

Given the newly recognized function of Maf1 in developmental programming, we asked whether it also played a role in modulating retinal development. We found that Maf1 was transiently expressed in most murine retinal progenitor cells (RPCs) and its targeted inactivation in mice diminished the retinal thickness and reduced the number of all retinal neuron types, which caused decreased electroretinogram (ERG) responses. The absence of *Maf1* led to aberrant differentiation of all retinal neuron types and decreased expression of their molecular markers; whereas it promoted RPC proliferation and increased RPC marker expression. As a result, *Maf1* inactivation caused substantial reduction in retinal neuron production despite elevated RPCs that subsequently degenerated by apoptosis. Genome-wide chromatin profiling and transcription assay showed that Maf1 bound broadly to the genome to negatively or positively regulate the expression of a large set of Pol II-transcribed genes involved in retinal proliferation, differentiation and/or survival. Our results together indicate that Maf1 may control the generation of correct number of neurons during retinal development by a balanced regulation of cell proliferation, differentiation, and death via both RNA Pol III-dependent and -independent mechanisms.

RESULTS

Pattern of *Maf1* expression during mouse retinal development

We carried out RNA in situ hybridization and immunofluorescence staining to investigate the spatiotemporal expression pattern of *Maf1* in the mouse retina at different developmental stages (Figure S1). At embryonic stages E12.5-E18.5, *Maf1 RNA* transcripts were distributed throughout the entire retina including both the RPCs in the outer neuroblastic layer and differentiating cells within the inner neuroblastic layer, with RNA in situ hybridization signals gradually concentrating in the inner neuroblastic layer (Figures S1A–S1D). From P0 to P8, *Maf1* transcripts gradually disappeared from the outer nuclear layer (ONL) while they were progressively limited to the inner nuclear layer (INL) and ganglion cell layer (GCL) (Figures S1E–S1G). And from P21 onward, strong *Maf1* RNA expression remained in the INL and GCL (Figure S1H).

Maf1 protein has a very similar expression pattern as its RNA transcript. At embryonic stages E12.5-E18.5, its immunoreactivity was detected in most RPCs in the outer neuroblastic layer and much stronger immunoreactivity was seen in differentiating cells in the inner neuroblastic layer (Figures S1I–S1L). At early postnatal stages, strong Maf1-immunoreactivity was found in the INL, GCL, and migrating horizontal cells while the outer neuroblastic layer gradually lost the Maf1-immunoreactivity (Figures S1M–S1O). In P21 and adult retinas, strong Maf1-immunoreactivity remained in the INL and GCL as well as in both outer and inner plexiform layers (Figure S1P). Therefore, Maf1 is transiently expressed in RPCs and then permanently expressed in most cells of the inner retina, hence displaying a dynamic spatiotemporal expression pattern during mouse retinal development.

By double immunolabeling, we found that Maf1 was co-expressed in more than 90% of Vsx2/Chx10$^+$ bipolar cells, Pax6$^+$ amacrine cells, GAD2/GAD65$^+$ GABAergic amacrine cells, Slc6a9/GLYT1$^+$ glycinergic amacrine cells, Calb1/calbindin$^+$ horizontal cells, Pou4f1/Brn3a$^+$ and Pou4f2/Brn3b$^+$ RGCs, or Glul$^+$ and Sox2$^+$ Müller cells (Figure S2). These results suggest that Maf1 may be expressed in all or nearly all cells located in the INL and GCL in the mature mouse retina. As mentioned in the following text, the spatiotemporal expression pattern of Maf1 protein in developing and adult retinas was further confirmed by the immunolabeling pattern of the tdTomato reporter knocked-in the *Maf1* locus (Figure S4).

Retinal dysfunction in *Maf1* null mutant mice

To investigate the role of *Maf1* during retinal development, we utilized the CRISPR/Cas9 gene-editing technology to create a *Maf1* knockout mouse line in which the coding part of exon 3 and all exon 4 was substituted by a tdTomato expression DNA sequence (Figure 1A). *Maf1* inactivation was confirmed by genotyping at the DNA level, qRT-PCR assay at the RNA level, and Western blotting/immunostaining at the protein level (Figures S3A–S3E). In developing and mature *Maf1*$^{+/-}$ animals, tdTomato expression was co-localized with Maf1 protein in the retina (Figure S3F), and essentially recapitulated the spatiotemporal expression pattern of Maf1 during embryonic and postnatal retinal development (Figure S4). The eyes of adult wild-type (WT) and *Maf1*$^{-/-}$ mice were grossly normal with the formation of similar lenses and corneas, and the transparency of their lenses was also indistinguishable when assayed in culture (Figure S5).

To characterize retinal deficiency in *Maf1* null mice, we first measured the retinal thickness in one-month-old WT and *Maf1*$^{-/-}$ mice by optical coherence tomography (OCT). Compared to the WT retina, we found that the null retina was overall thinner and in particular, significantly thinner in the central region (Figures 1B–1D). We then quantified HE (hematoxylin-eosin)-stained nuclei in different retinal layers and found that there was an approximately 11.3%, 13.7%, and 20.1% reduction in the number of nuclei within the ONL, INL, and GCL of the null retina, respectively, compared to those of the WT retina (Figures 1E–1I). These results indicate that there may be loss of multiple cell types in the mature *Maf1* null retina.

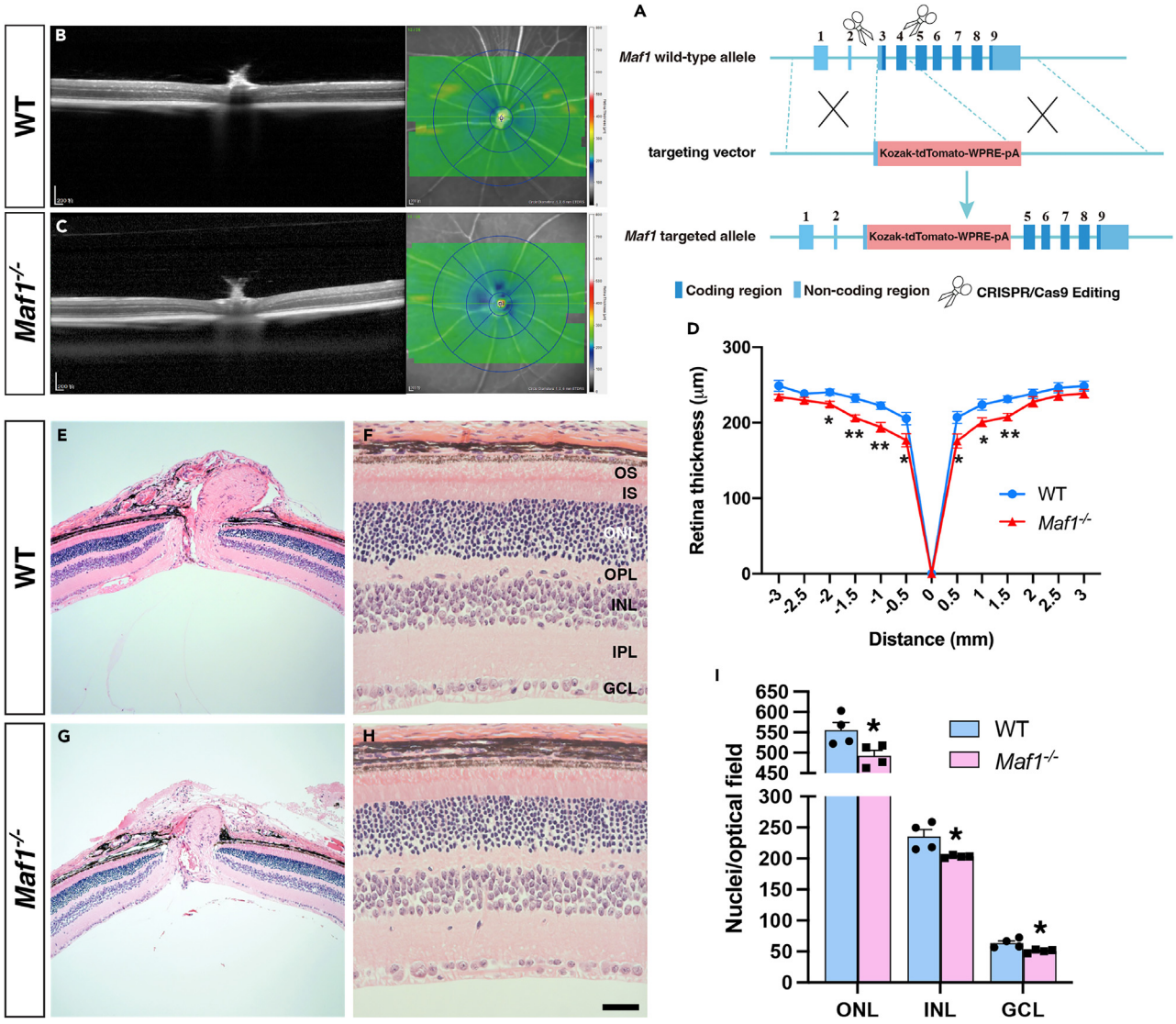

Figure 1. Reduced retinal thickness and cell number in *Maf1*$^{-/-}$ mice

(A) Schematic diagram illustrating targeted disruption of the *Maf1* locus in mice. By CRISPR/Cas9 gene editing, the great majority of exon 3 and all exon 4 were substituted by a tdTomato expression sequence.

(B and C) OCT (optical coherence tomography) images of retinas from one-month-old wild-type (WT) and *Maf1*$^{-/-}$ mice.

(D) OCT measurement of retinal thickness from the optic disc to peripheral regions. Each point represents the mean ± SEM for 9 or 10 retinas. *$p < 0.05$; **$p < 0.01$.

(E–H) Retinal laminar structures of one-month-old WT and *Maf1*$^{-/-}$ mice were visualized by HE (hematoxylin-eosin) staining of retinal sections.

(I) The number of nuclei in the ONL, INL, and GCL of WT and *Maf1*$^{-/-}$ retinas were counted and presented as mean ± SEM (n = 4). *$p < 0.05$. Abbreviations: GCL, ganglion cell layer; INL, inner nuclear layer; IPL, inner plexiform layer; IS, inner segment; ONL, outer nuclear layer; OPL: outer plexiform layer; OS, outer segment. Scale bar: E,G, 80 μm; F,H, 20 μm.

To assess whether the observed cell loss in *Maf1* null retinas would impair visual function, we recorded scotopic electroretinogram (ERG) responses in WT and *Maf1*$^{-/-}$ mice aged at 2 and 6 months. Under dark-adapted condition and all tested low and high flash intensities (0.003–10.0 cd s/m^2), substantial reductions in scotopic b-wave amplitudes (~34% on average) were observed in mutants of both ages compared to control animals (Figures 2A, 2C, 2E). Moreover, the response amplitudes of a-waves elicited from mutant animals were also decreased by ~26% on average for flash intensities 0.1 cd s/m^2 and above (Figures 2A, 2B, and 2D). Similar to scotopic ERG responses, *Maf1*$^{-/-}$ mice also exhibited a decrease in amplitudes of both a- and b-waves of light-adapted ERG responses, albeit with statistical significance only under high flash intensities (10.0 and/or 30.0 cd s/m^2) (Figure S6). In addition, compared to WT mice, oscillatory potentials (OPs) in scotopic ERG responses at 3.0 cd s/m^2 were reduced by up to 32.1% in *Maf1*$^{-/-}$ animals (Figure 2F). Because the a- and b-waves are primarily generated

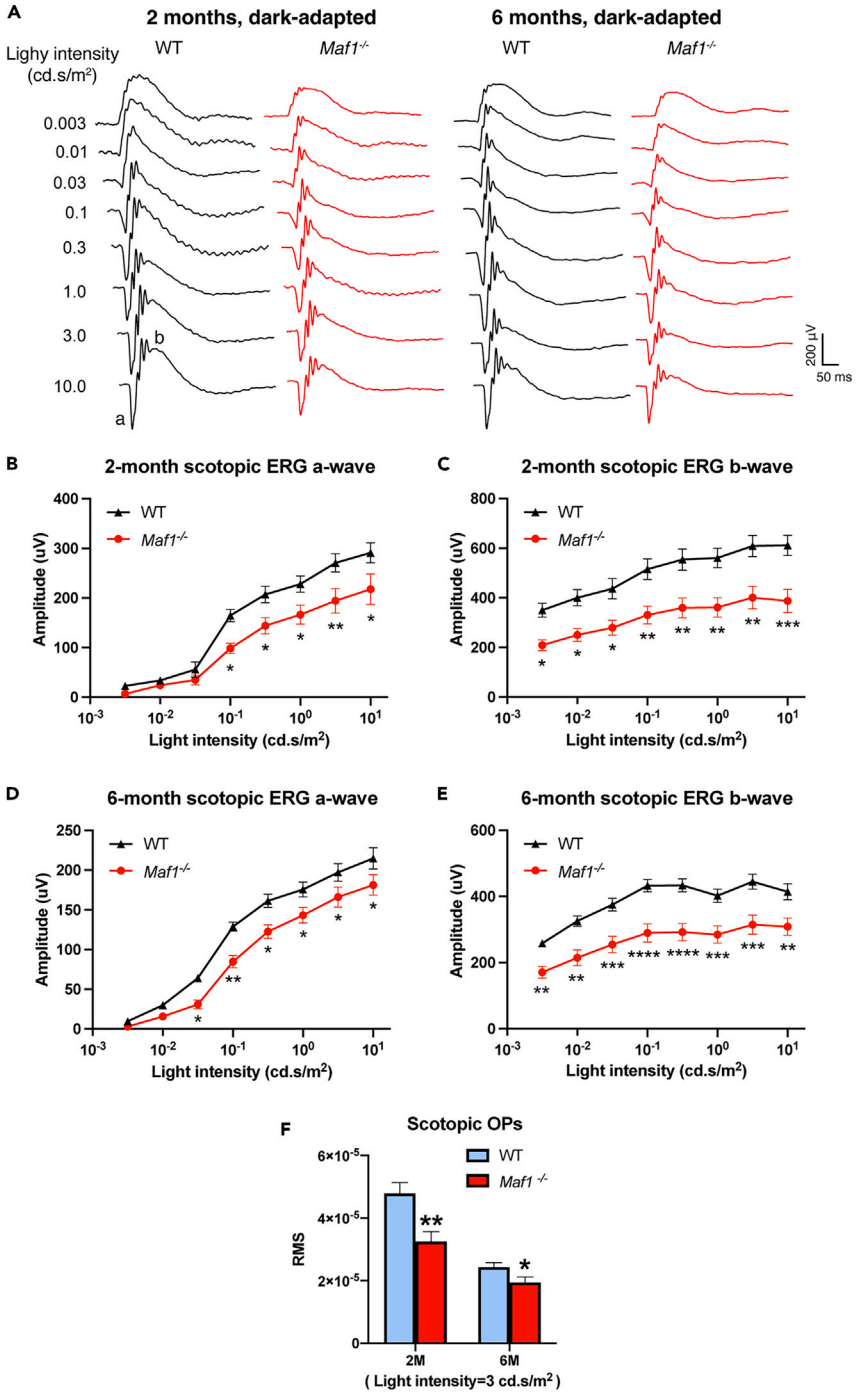

Figure 2. Decreased scotopic ERG (electroretinogram) responses of *Maf1*$^{-/-}$ mice

(A) Representative ERG waveforms from dark-adapted WT and *Maf1* mutant animals aged 2 and 6 months. The flash intensity used to elicit the responses is given to the left of each pair of responses.

(B–E) Intensity–response functions of scotopic ERG a waves (B and D) and b waves (C and E) for control and *Maf1* mutant mice aged 2 and 6 months. Data are presented as mean ± SEM (n = 6–10). Asterisks indicate significance in a two-way ANOVA test with the Holm-Sidak correction. *p < 0.05, **p < 0.01, ***p < 0.001, ****p < 0.0001.

(F) Oscillatory potentials (OPs) in ERG at 3 cd s/m^2. OP amplitudes were quantified using root-mean-square (RMS) for two-frequency bands in eight horizontal and seven vertical locations. Data are presented as mean ± SEM (n = 6–10). *p < 0.05, **p < 0.01.

by photoreceptors and bipolar cells, respectively, and OPs reflect the interaction among inner retinal neuron types including amacrine cells, bipolar cells, and RGCs,[35–37] their reduction suggests that *Maf1* inactivation may cause defects in all these cell types, consistent with cell loss observed in all retinal cellular layers of *Maf1* null mice. Additionally, ERG responses of *Maf1*$^{-/-}$ animals did not deteriorate with age from 2 to 6 months, suggesting that *Maf1* disruption may not cause retinal degeneration.

Loss of neuronal cell types in *Maf1* null retinas

To confirm that *Maf1* inactivation leads to loss of multiple retinal cell types, we compared the expression levels of a series of neuronal and glial (Müller) cell marker genes between WT and *Maf1*$^{-/-}$ retinas by qRT-PCR analysis. Compared to 1-month-old WT retinas, in *Maf1*$^{-/-}$ retinas, there was an approximately 10–20% decrease in expression levels of photoreceptor marker genes *Rcvrn* and *Crx*, rod marker genes *Rho*, *Gnat1*, and *Nrl*, cone marker genes *Arr3* and *Opn1sw*, bipolar cell marker genes *Vsx2* and *Prkca*, RGC marker genes *Rbpms* and *Pou4f1*, amacrine cell marker genes *Tfap2a* and *Gad1*, and horizontal cell marker genes *Lhx1* and *Calb1* (Figure 3A). However, there was no significant expression change in Müller glia cell marker genes *Sox9*, *Glul*, and *Rlbp1* (Figure 3A), indicating that all neuronal cell types display cell loss whereas Müller cells do not in the *Maf1* null retina.

We further validated neuronal cell type loss in *Maf1* null retinas by immunofluorescent staining with antibodies against a variety of cell type-specific protein markers. Quantification of immunoreactive cells in the intermediate retina revealed that in *Maf1*$^{-/-}$ retinas, the number of Vsx2^{+} bipolar cells and Prkca/PKCα^{+} rod bipolar cells was decreased by 32.4% and 28.4%, respectively, compared to the WT retina (Figures 3C, 3D, 3C′,3D′, and 3K). Similarly, the number of Tfap2a^{+} amacrine cells was reduced by 18.7% (Figures 3G, 3G′, and 3K). In agreement with the loss of these two cell types, Bhlhe22/Bhlhb5-immunoreactive type 2 OFF-cone bipolar cells and GABAergic amacrine cells were decreased by 29.7% (Figures 3E, 3E′, and 3K). There was also 6.7%, 17.3%, and 13.6% decrease in the number of cone arrestin-positive (Arr3^{+}) cones, Rbpms^{+} RGCs, and Lhx1^{+} horizontal cells, respectively (Figures 3B, 3H, 3I, 3B′, 3H′, 3I′, and 3K). Immunoreactivity for Pax6, a marker for amacrine cells, horizontal cells, and RGCs, was also visibly diminished in the mutant retina (Figures 3F and 3F′). However, there was no significant alteration in the number of Sox9^{+} Müller cells (Figures 3J, 3J′, and 4K). To minimize the effect of retinal geometric locations on cell number,[38–41] we quantified cells in the nasal, temporal, dorsal, and ventral quadrants of the intermediate region in WT and *Maf1*$^{-/-}$ retinal wholemounts and observed a similar decrease in these quadrants of null retinas for Arr3^{+} cones, Vsx2^{+} bipolar cells, Tfap2a^{+} amacrine cells, and Rbpms^{+} RGCs (Figure S7). These results together thus suggest that the absence of *Maf1* may result in cell loss in all 6 retinal neuron types including rod, cone, bipolar, ganglion, amacrine, and horizontal cells but have no effect on Müller glial cells.

Differentiation defects of neuronal cell types in developing *Maf1* null retinas

Given that the majority of cells of all 6 neuronal types are present in adult *Maf1* null retinas, Maf1 is unlikely required for specifying the fates of retinal neuron cell types. We therefore sought to determine whether Maf1 would affect their differentiation first by bulk RNA-seq analysis of WT and *Maf1*$^{-/-}$ retinas at P0 and P8 when amacrine, rod, and bipolar cells are still undergoing generation and initial differentiation and ganglion, cone, and horizontal cells are undergoing late differentiation. This analysis yielded a group of downregulated genes as well as a cluster of upregulated genes in *Maf1*$^{-/-}$ retinas at both postnatal stages (Figure S8; Tables S1 and S2). The downregulated genes were enriched for GO (gene ontology) terms associated with retinal neuron functions such as axonogenesis, synapse organization, neuron projection guidance, monoamine transport, phototransduction, and response to light stimulus (Figures 4A and 4B), implicating a defect in neuronal cell differentiation in *Maf1*$^{-/-}$ retinas. Expression heatmaps showed that a large number of RGC marker genes were downregulated in *Maf1*$^{-/-}$ retinas compared to control ones at P0 (Figure 4C). Similarly, in P8 null mutant retinas, many bipolar cell marker genes, rod and cone marker genes, and amacrine and horizontal cell marker genes were all downregulated (Figures 4E–4G). Among the downregulated genes were a number of transcription factor (TF) genes including *Atoh7*, *Pou4f1-3*, *Ebf1-4*, *Isl1*, *Vsx2*, *Bhlhe23*, *Crx*, *Nrl*, *Nr2e3*, *Prox1*, *Prdm13*, *Tfap2a*, *Tfap2b*, *Sall3*, and *Lhx1* (Figures 4C, 4E–4G), which have been demonstrated to be involved in the differentiation of ganglion, bipolar, rod, cone, amacrine, and/or horizontal cells. qRT-PCR assay confirmed significant downregulation in expression of RGC marker genes *Rbpms*, *Pou4f1*, *Pou4f2*, and *Irx5*, amacrine and/or horizontal marker genes *Tfap2a*, *Calb1*, and *Lhx1*, and rod and/or cone marker genes *Rcvrn* and *Opn1sw* in P0 *Maf1*$^{-/-}$ retinas (Figure 4D). In P8 *Maf1*$^{-/-}$ retinas, there were similar downregulation in expression of bipolar cell marker genes *Vsx2*, *Prkca*, *Bhlhe23*, and *Car8*, rod marker genes *Rho* and *Rcvrn*, and cone marker genes *Arr3* and *Opn1sw* (Figure 4H). By contrast, we did not detect significant change in expression of Müller cell marker genes *Glul* and *Rlbp1* (Figure 4H). These results suggest that *Maf1* inactivation may cause defective differentiation in all 6 retinal neuron types, perhaps by downregulating the expression of relevant regulatory TF genes.

Single-cell transcriptomics is able to reveal cell lineage trajectories during retinal development.[42] We thus performed scRNA-seq analyses of P3 and P7 WT and *Maf1*$^{-/-}$ retinas to evaluate possible differentiation defects in cell lineage trajectories. After removing doublet cells, microglia, astrocytes, and endothelial cells as well as performing a random downsampling, we obtained expression data of 7,854 cells each for P3 WT and *Maf1*$^{-/-}$ retinas and 8,007 cells each for P7 WT and *Maf1*$^{-/-}$ retinas. Unsupervised combined with marker-based UMAP clustering was conducted using Seurat 4[43] on these cells, which resulted in 9 clusters (c1-c9) each for P3 and P7 cells (Figures 5A, 5D, S9A, and S9B). At P3, the transitional retinal progenitor cells (tRPCs), which originated from the naive RPCs (nRPCs), gave rise to two cell lineage trajectories: the amacrine cell trajectory consisting of clusters c3-c5 and the rod cell trajectory composed of clusters c7 and c8 (Figures 5A and S9A). Although both the amacrine and rod trajectories were formed in WT and null retinas, the terminal clusters of the two trajectories (c5 and c8), which developmentally advanced most as determined by pseudotime trajectory analysis (Figure S9C), exhibited cell loss whereas the RPC clusters (c1 and c2) displayed no such cell loss in null retinas (Figures 5B and 5C). As expected, there was cell loss in

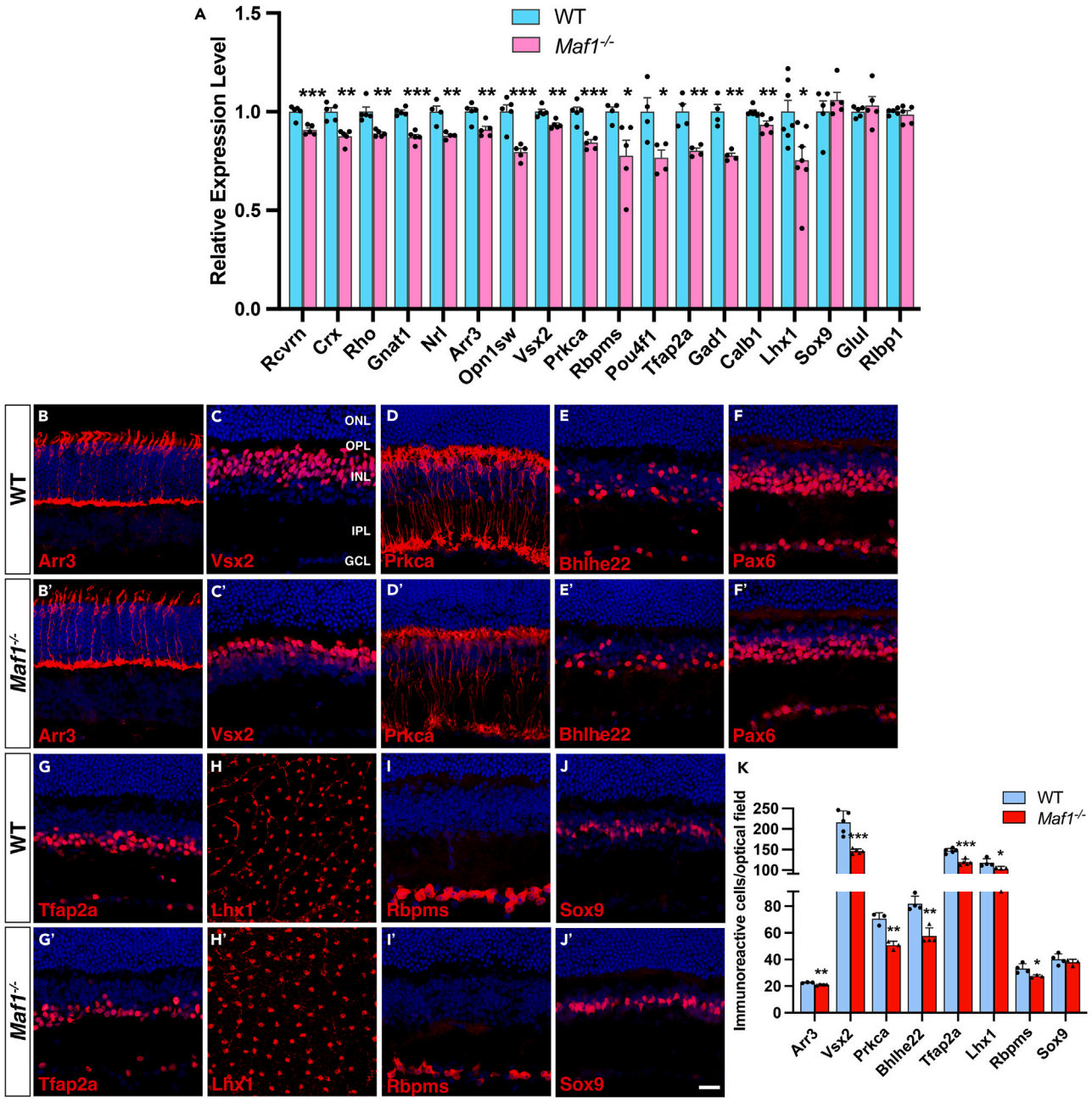

Figure 3. Loss of neuronal cell types in *Maf1*$^{-/-}$ retinas

(A) The expression levels of a series of neuronal and Müller cell marker genes in WT and *Maf1*$^{-/-}$ retinas were determined by qRT-PCR analysis. Each histogram represents the mean ± SEM (n = 5–7). *p < 0.05, **p < 0.01, ***p < 0.001.

(B–J and B′–J′) Retinal sections (B–G, I,J,B′–G′, and I′,J′) and wholemounts (H and H′) from one-month-old WT and *Maf1*$^{-/-}$ mice were immunostained with antibodies against the indicated cell type-specific markers. All sections were also counterlabeled with nuclear DAPI. *Maf1* inactivation resulted in a decrease of cone cells immunoreactive for Arr3 (B and B′), bipolar cells immunoreactive for Vsx2, Prkca, or Bhlhe22 (C–E and C′–E′), amacrine cells immunoreactive for Bhlhe22, Pax6, or Tfap2a (E–G and E′–G′), horizontal cells immunoreactive for Lhx1 (H and H′), and RGCs immunoreactive for Rbpms (I and I′); but no obvious change in Sox9^{+} Müller cells (J and J′).

(K) Quantitation of cells that are immunoreactive for several cell type-specific markers. Each histogram represents the mean ± SEM for 3–5 retinas. *p < 0.05, **p < 0.01, ***p < 0.001. GCL, ganglion cell layer; INL, inner nuclear layer; IPL, inner plexiform layer; ONL, outer nuclear layer; OPL, outer plexiform layer. Scale bar: B–G,I,J,B′–G′,I′, and J′, 20 μm; H,H′, 40 μm.

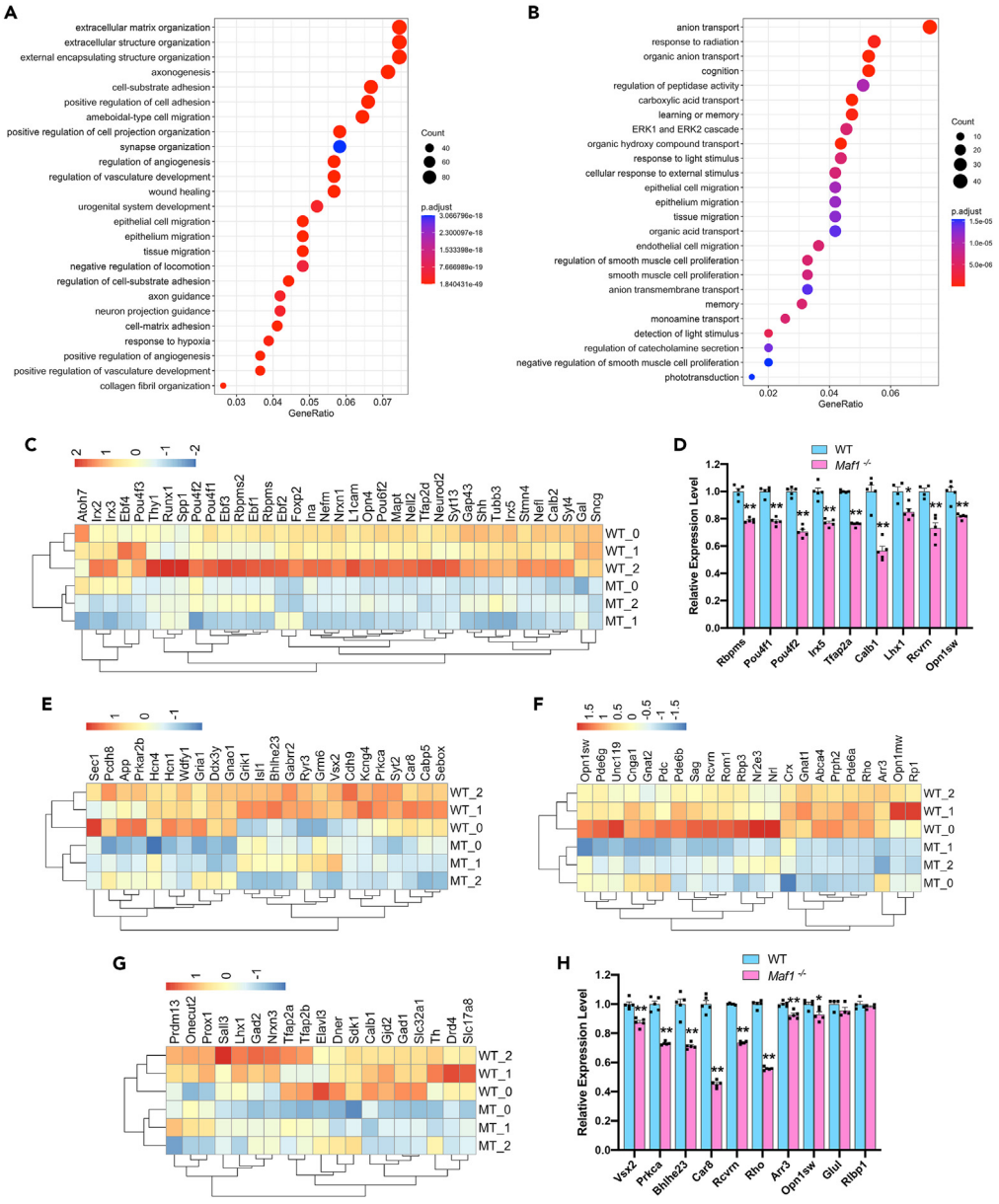

Figure 4. Altered transcriptomes in P0 and P8 *Maf1*$^{-/-}$ retinas revealed by bulk RNA-seq analyses

(A and B) GO (gene ontology) term enrichment analyses of downregulated genes in *Maf1*$^{-/-}$ retinas at P0 (A) and P8 (B).

(C) Heatmap of expression levels of a set of RGC marker genes in P0 WT and mutant (MT) retinas.

(D) qRT-PCR assay of the RNA expression levels of the indicated cell type-specific marker genes in P0 WT and *Maf1*$^{-/-}$ retinas. Data are presented as mean ± SEM (n = 4 or 5). *p < 0.01, **p < 0.001.

(E–G) Heatmaps of expression levels of a set of bipolar cell marker genes (E), rod and cone marker genes (F), and amacrine and horizontal cell marker genes (G) in P8 WT and mutant retinas.

(H) qRT-PCR assay of the RNA expression levels of the indicated cell type-specific marker genes in P8 WT and *Maf1*$^{-/-}$ retinas. Data are presented as mean ± SEM (n = 4 or 5). *p < 0.05, **p < 0.001.

the more mature cone cluster (c6) and RGC cluster (c9) (Figures 5A–5C and S9A). There were also two cell lineage trajectories at P7: the rod cell trajectory (c5-c7) and bipolar cell one (c3 and c4) (Figures 5D and S9B). Similarly, the two branches of lineage trajectories were largely intact in P7 null retinas and the intermediate clusters (c3, c5, and c6) displayed no cell loss (Figures 5E and 5F), indicating that *Maf1* inactivation may have no effect on the determination of rod and bipolar cell fates. By contrast, the cell number was decreased in the two terminal clusters (c4 and c7) as well as in the more mature cone cluster (c8) and amacrine cell cluster (c9) (Figures 5D–5F), consistent with a defect in early differentiation of rod, cone, bipolar, and amacrine cells.

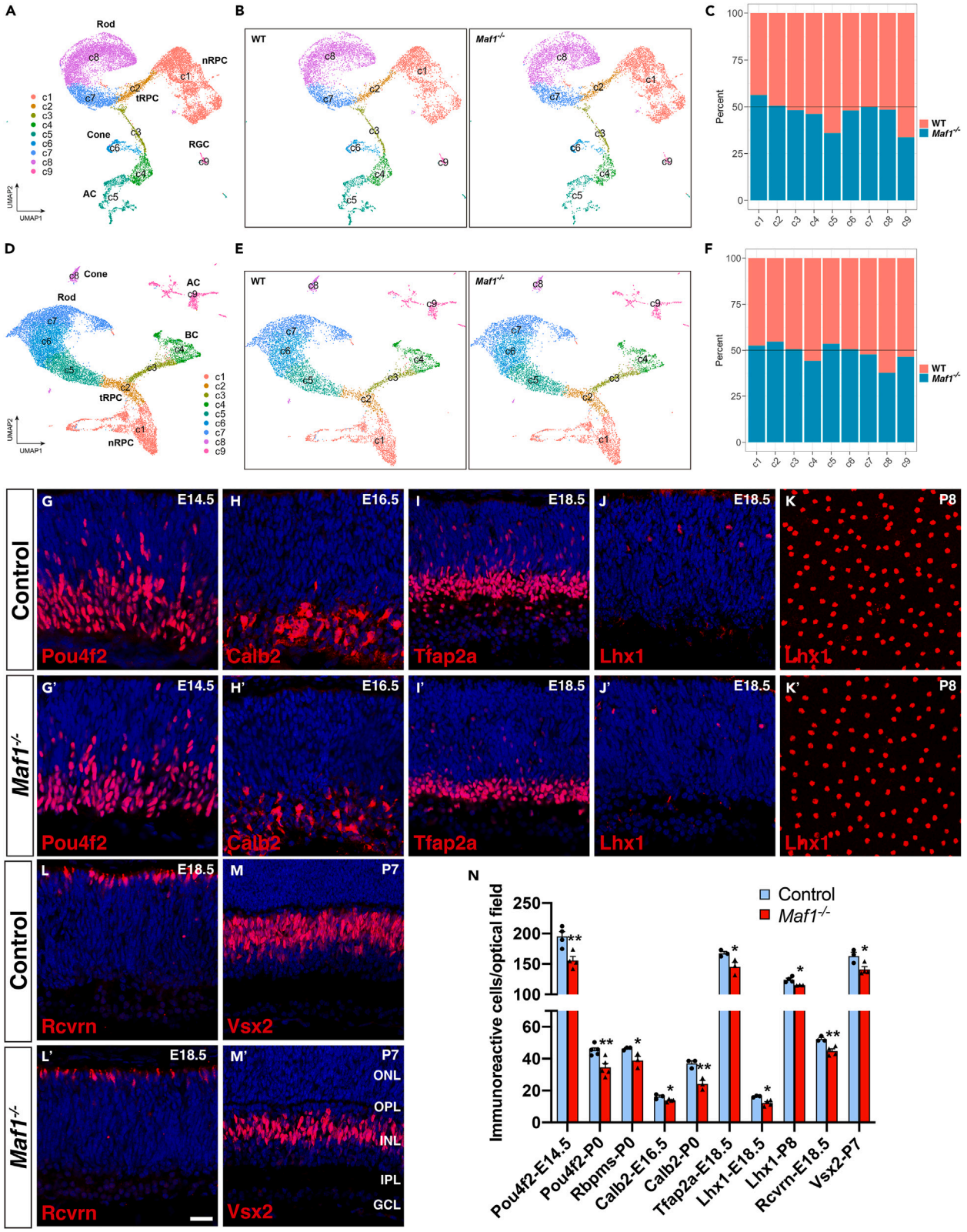
A
Rod
nRPC
tRPC
Cone
RGC
AC
c1
c2
c3
c4
c5
c6
c7
c8
c9
UMAP2
UMAP1
B
WT
Maf1-/-
C
Percent
100
75
50
25
0
WT
Maf1-/-
D
Cone
AC
Rod
BC
tRPC
nRPC
E
WT
Maf1-/-
F
Percent
WT
Maf1-/-
Control
Maf1-/-
G E14.5 Pou4f2
H E16.5 Calb2
I E18.5 Tfap2a
J E18.5 Lhx1
K P8 Lhx1
G' E14.5 Pou4f2
H' E16.5 Calb2
I' E18.5 Tfap2a
J' E18.5 Lhx1
K' P8 Lhx1
L E18.5 Rcvrn
M P7 Vsx2
L' E18.5 Rcvrn
M' P7 Vsx2
ONL
OPL
INL
IPL
GCL
N
Control
Maf1-/-
Immunoreactive cells/optical field
250
200
150
100
60
40
20
0
Pou4f2-E14.5
Pou4f2-P0
Rbpms-P0
Calb2-E16.5
Calb2-P0
Tfap2a-E18.5
Lhx1-E18.5
Lhx1-P8
Rcvrn-E18.5
Vsx2-P7

Figure 5. Cell differentiation defects in developing *Maf1*$^{-/-}$ retinas

(A) UMAP plot of single cells from P3 WT and *Maf1*$^{-/-}$ retinas resulting from unsupervised combined with marker-based clustering analysis.

(B) Comparison of UMAP plots of equal number of single cells from P3 WT and *Maf1*$^{-/-}$ retinas.

(C) Proportion of cell number in each cluster in P3 WT and *Maf1*$^{-/-}$ retinas.

(D) UMAP plot of single cells from P7 WT and *Maf1*$^{-/-}$ retinas resulting from unsupervised combined with marker-based clustering analysis.

(E) Comparison of UMAP plots of equal number of single cells from P7 WT and *Maf1*$^{-/-}$ retinas.

(F) Proportion of cell number in each cluster in P7 WT and *Maf1*$^{-/-}$ retinas.

(G and G′) Retinal sections from E14.5 control and *Maf1*$^{-/-}$ mice were immunostained for the RGC marker Pou4f2.

(H and H′) Retinal sections from E16.5 control and *Maf1*$^{-/-}$ mice were immunostained for Calb2, a marker for RGCs and amacrine cells.

(I and I′) Retinal sections from E18.5 control and *Maf1*$^{-/-}$ mice were immunostained for the amacrine cell marker Tfap2a.

(J, K, J′, and K′) E18.5 retinal sections (J and J′) and P8 retinal flatmounts (K and K′) from control and *Maf1*$^{-/-}$ mice were immunostained for the horizontal cell marker Lhx1.

(L and L′) Retinal sections from E18.5 control and *Maf1*$^{-/-}$ retinas were immunostained for the photoreceptor marker Rcvrn.

(M and M′) Retinal sections from P7 control and *Maf1*$^{-/-}$ retinas were immunostained for the bipolar cell marker Vsx2.

(N) Quantitation of cells that are immunoreactive for several cell type-specific markers at different developmental stages. Each histogram represents the mean ± SEM for 3–5 retinas. *p < 0.05, **p < 0.01. All retinal sections were counterstained with nuclear DAPI. GCL, ganglion cell layer; INL, inner nuclear layer; IPL, inner plexiform layer; ONL, outer nuclear layer; OPL, outer plexiform layer. Scale bar: G–J, L, M, G′–J′, L′, and M′, 20 μm; K and K′, 40 μm.

In the P7 scRNA-seq dataset, consistent with the bulk RNA-seq data and neuron differentiation deficit, the average expression levels of many photoreceptor, bipolar, and amacrine cell marker genes were downregulated in *Maf1* null retinas (Figure S10A). However, as revealed by violin and feature plots, there was no obvious difference in single-cell expression levels between WT and null retinas for bipolar cell marker genes *Isl1*, *Bhlhe23*, *Vsx1*, and *Grik1* in cluster c4, cone marker genes *Rcvrn*, *Opn1sw*, *Arr3*, and *Gnat2* in cluster c8, and amacrine cell marker genes *Tfap2b*, *Prdm13*, *Nrxn1*, and *Dner* in cluster c9 (Figure S10B–S10E). To better resolve single cells in these clusters, we separately re-analyzed clusters c4, c8, and c9 by UMAP clustering. Feature plots of gene expression in these clusters further showed that the marker gene expression levels in single cone, bipolar, and amacrine cells did not display overt difference between WT and *Maf1* null retinas but there were fewer cone, bipolar, and amacrine cells in the null retina (Figures S10F–S10Q). Therefore, in agreement with the aforementioned marker immunostaining results, the differentiation defects resulting from *Maf1* inactivation appear to primarily cause retinal neuron loss rather than mis-differentiation of retinal neurons with decreased marker gene expression.

We confirmed neuronal differentiation defects in developing *Maf1* null retinas by immunostaining for cell type-specific protein markers. In E14.5, E16.5, and E18.5 *Maf1*$^{-/-}$ retinas, compared to the control, we detected 13.2–25.6% decrease in the number of Pou4f2^{+} RGCs, Calb2^{+} (calretinin^{+}) RGCs/amacrine cells, Tfap2a^{+} amacrine cells, Lhx1^{+} horizontal cells, or Rcvrn^{+} cone cells, and this reduction continued at stages P0 and P8 (Figures 5G–5L, 5G′–5L′, and 5N). In addition, there was a significant decrease of Rbpms^{+} RGCs in P0 null retinas (Figure 5N). Consistent with this, we observed reduced Rbpms- and Calb2-immunoreactivity in *Maf1*$^{-/-}$ retinas at E14.5, E16.5, E18.5, and P0 (Figure S11). Since most RGCs and amacrine, horizontal and cone photoreceptor cells are being generated and differentiating during embryogenesis,[12] these results suggest that the absence of *Maf1* leads to a deficiency in the differentiation of RGCs and amacrine, horizontal, and photoreceptor cells. In contrast, most bipolar cells are being generated and differentiating in the first postnatal week.[12] We thus detected 13.9–24.1% decrease in the number of Vsx2^{+} bipolar cells in P7, P8, and P12 null retinas (Figures 5M, 5M′, 5N, and S12).

Increased progenitor cell proliferation in developing *Maf1* null retinas

Maf1 is known to inhibit cell proliferation by repressing the activity of RNA Pol III which is responsible for the transcription of pre-tRNAs, 5S rRNA, and other small RNAs. We thus investigated whether *Maf1* inactivation would affect Pol III-dependent transcription and RPC proliferation. By qRT-PCR assay, we observed in *Maf1*$^{-/-}$ retinas dramatic upregulation in expression of *tRNA*^{Met}, *tRNA*^{Leu}, *5S rRNA* (*Rn5s*), and *U6 RNA* (*Rnu6*) (Figure S13), consistent with the fact that Maf1 acts as a strong Pol III inhibitor. By contrast, in *Maf1* null retinas, there were only minimal changes in expression levels of Pol I-dependent transcripts 18S and 28S rRNA or constitutively expressed Pol II-dependent transcripts *Gapdh* and *Hist3h2a* (Figure S13B). To evaluate the effect of enhanced Pol III transcription on RPC proliferation, we first performed a GO enrichment analysis of the upregulated genes in P0 *Maf1*$^{-/-}$ retinas identified by bulk RNA-seq analysis. This revealed that the upregulated genes were primarily enriched for GO terms associated with cell cycle such as positive regulation of cell cycle, mitotic nuclear division, sister chromatid segregation, spindle organization, and ribosome biogenesis (Figure 6A). Expression heatmaps further showed that there was an upregulation in expression of a large set of S-phase marker genes and G2/M-phase marker genes in P0 null retinas (Figures 6B and 6C), indicating an increase of RPC proliferation in *Maf1*$^{-/-}$ retinas. We then carried out a cell cycle analysis of the sequenced single cells of P3 control and null retinas by Seurat using 70 cell cycle markers.[44] This analysis revealed an obvious increase in the number of S and G2/M nRPCs (in the c1 cluster) in P3 *Maf1*$^{-/-}$ retinas compared to the WT control (Figures 6D and 6E). Consistent with enhanced cell proliferation, there were indeed more nRPCs (c1 cells) in P3 and P7 *Maf1*$^{-/-}$ retinas (Figures 5A–5F).

We confirmed increased RPC proliferation in *Maf1*$^{-/-}$ embryonic and postnatal retinas by immunostaining with an antibody against phosphorylated histone H3 (pH3), an M-phase marker, as well as by short pulse-labeling with EdU, an S-phase marker. We found that in *Maf1*$^{-/-}$ retinas, pH3-immunoreactive cells were increased consistently at all tested stages including E14.5, E16.5, E18.5, P0, and P4 (Figures 6F–6J, 6F′–6J′, and 6L); Similarly, EdU-positive cells were increased by ~15.1% in E18.5 null retinas (Figures 6K, 6K′, and 6M), consistent with the increased mitotic progenitors in S and G2/M phases as well as upregulated expression of S and G2/M marker genes revealed by bulk

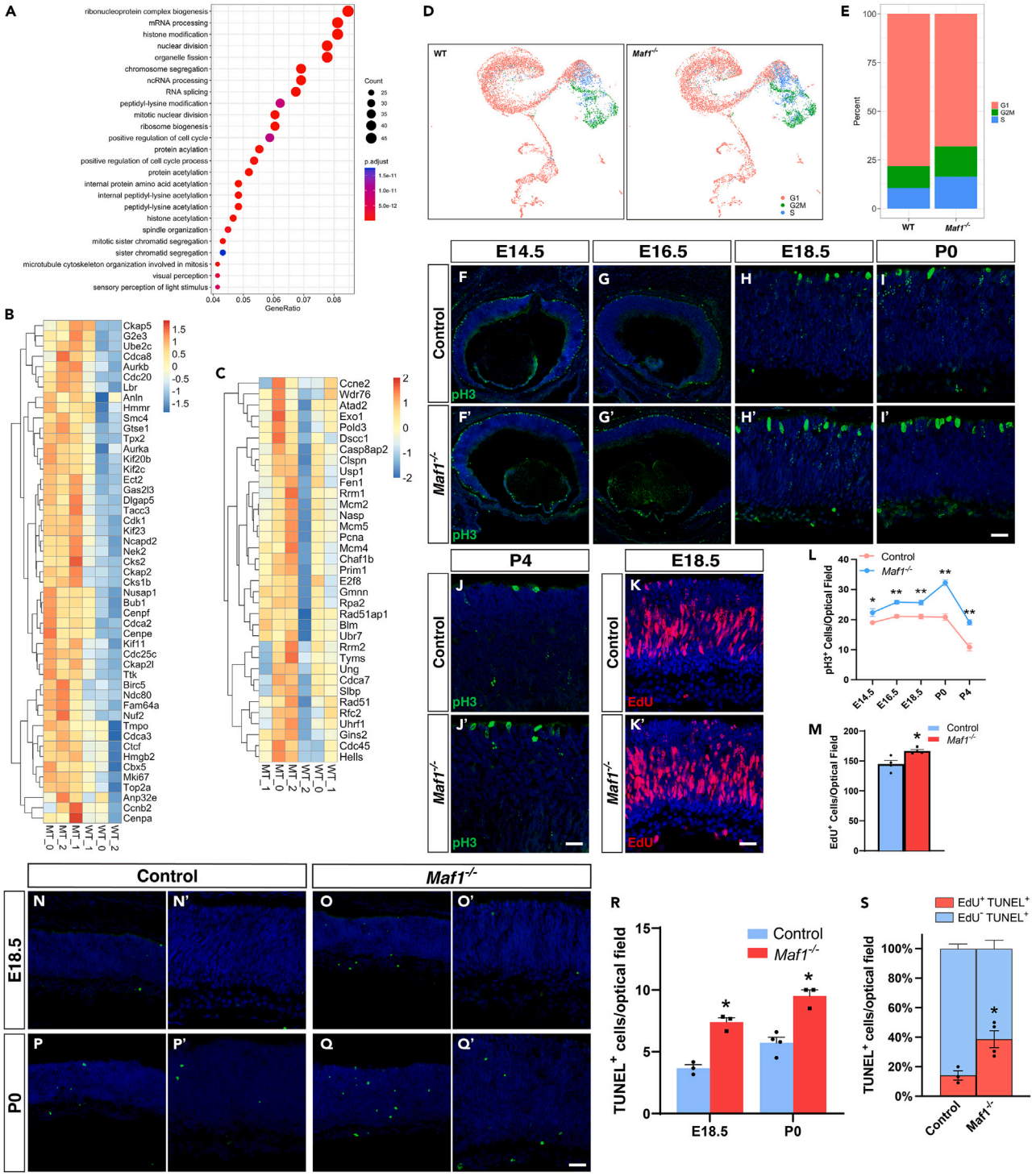

Figure 6. Enhanced retinal progenitor proliferation in *Maf1*$^{-/-}$ mice

(A) GO term enrichment analysis of upregulated genes in P0 *Maf1*$^{-/-}$ retinas.

(B and C) Heatmaps of expression levels of a set of G2/M-phase marker genes (B) and S-phase marker genes (C) in P0 WT and mutant (MT) retinas.

(D and E) Cell cycle analysis showing an increase in the proportion of cells distributed in S and G2/M phases in P3 *Maf1*$^{-/-}$ retinas.

(F–J and F′–J′) Retinal sections from the indicated developmental stages were immunolabeled with an anti-pH3 (phosphorylated histone H3) antibody and counterstained with DAPI. There were more pH3-positive cells in *Maf1*$^{-/-}$ retinas than those in controls at these stages.

Figure 6. *Continued*

(K and K′) RPCs in S phase in E18.5 control and *Maf1*$^{-/-}$ retinas were pulse-labeled by EdU and then visualized in sections by fluorescence staining for EdU with DAPI counterlabeling.

(L) Quantitation of pH3^{+} cells in control and *Maf1*$^{-/-}$ retinas at the indicated developmental stages (E14.5-P4). Each point represents the mean ± SEM for 3 or 4 retinas. *p < 0.05, **p < 0.001.

(M) Quantitation of EdU^{+} cells in E18.5 control and *Maf1*$^{-/-}$ retinas. Each histogram represents the mean ± SEM for 4 retinas. *p < 0.05.

(N–Q and N′–Q′) Cells undergoing apoptosis were TUNEL-labeled and counterstained with DAPI in E18.5 and P0 control and *Maf1*$^{-/-}$ retinal sections.

(R) Quantitation of TUNEL^{+} cells in E18.5 and P0 control and *Maf1*$^{-/-}$ retinas. Each histogram represents the mean ± SEM for 3 or 4 retinas. *p < 0.005.

(S) Percentage of EdU^{+} and EdU^{-} cell populations among total TUNEL^{+} cells in E18.5 control and *Maf1*$^{-/-}$ retinas. Each histogram represents the mean ± SEM for 3 or 4 retinas. *p < 0.05. Scale bar: F,G,F′, and G′, 80 μm; N-Q,40 μm; H–K, H′–K′, and N′–Q′, 20 μm.

RNA-seq and scRNA-seq analyses (Figures 6B–6E). Despite this elevation, however, *Maf1* inactivation did not appear to prolong the duration of RPC proliferation during development since EdU-positive cells disappeared in both control and *Maf1*$^{-/-}$ retinas by P11 (Figure S14). To ascertain whether the increased mitotic RPCs might result from altered cell cycle dynamics, we utilized a BrdU/EdU dual labeling approach[45–47] to determine RPC cell cycle kinetic parameters in E14 WT and *Maf1*$^{-/-}$ retinas (Figure S15A). Based on the number of EdU, BrdU, or Ki67 positive cells (Figures S15B–S15G), we were able to calculate the total cell cycle length (Tc) and the S-phase length (Ts) (Figures S15H and S15I). The results revealed that *Maf1*$^{-/-}$ RPCs had a Tc that was 24.7% shorter than that of WT RPCs (17.02 vs. 22.60 h) and that their Ts was also 21.7% shorter (Figures S15H and S15I), suggesting that the absence of *Maf1* may shorten the RPC cell cycle length, which would lead to increased RPCs.

Given the substantial loss of neuronal cells in adult *Maf1*$^{-/-}$ retinas, the superfluous RPCs resulting from enhanced proliferation during development did not appear to differentiate into mature neurons. To test whether they were eliminated by cell death, we labeled apoptotic cells in mutant and control retinal sections by TUNEL (terminal deoxynucleotidyl transferase-mediated nick end labeling). Compared to control retinas, TUNEL^{+} cells were increased by 101.5% at E18.5 and by 65.9% at P0 in *Maf1*$^{-/-}$ retinas (Figures 6N–6Q, 6N′–6Q′, and 6R). RPCs exist mainly in the periphery of the retina at later postnatal stages (Figure S14). So we quantified TUNEL^{+} cells in the peripheral region at P6-P8, which revealed a significant increase of 165.1% and 107.8%, respectively, in TUNEL^{+} cells in P6 and P7 *Maf1*$^{-/-}$ retinas compared to controls (Figures S16A–S16D, S16A′–S16D′, and S16G). P8 *Maf1*$^{-/-}$ retinas showed an increase of TUNEL^{+} cells without reaching significance (Figures S12E–S12G, S12E′, and S12F′). To directly visualize the death of superfluous RPCs, we carried out EdU and TUNEL double-labeling of E18.5 control and *Maf1*$^{-/-}$ retinal sections and observed a 173.6% increase of EdU^{+}TUNEL^{+} double-positive cells in the null retina (Figure 6S and S17). These results thus suggest that excessive RPCs resulting from *Maf1* inactivation may be eventually eliminated by apoptosis.

Failure to rescue neuron differentiation defects in *Maf1* null retinas by Pol III inhibition

Maf1 inactivation leads to enhanced Pol III activity which in turn may cause defect in retinal neuron differentiation. To test this possibility, we performed a rescue experiment in which P0 *Maf1*$^{-/-}$ retinal explants were cultured in the presence of a Pol III-specific chemical inhibitor ML-60218,[33] and collected at day 10 for qRT-PCR analysis (Figure 7A). Judged by *tRNA*^{Met} expression levels, the greatly elevated Pol III activity resulting from *Maf1* inactivation was brought down to a level close to that of WT retinas by treatment with 20 μM ML-60218 (Figure 7B). Despite this reduction of Pol III-dependent transcription, ML-60218 treatment of *Maf1*$^{-/-}$ explants did not result in any significant increase in expression of bipolar cell marker genes *Vsx2* and *Prkca*, or amacrine cell marker genes *Tfap2a*, *Gad1*, and *Calb2* (Figure 7B). Since both cell types are being generated and undergoing initial differentiation in the early postnatal period, these results suggest that the neuronal differentiation phenotype caused by *Maf1* inactivation may not be rescued by Pol III inhibition and thus may in part result from a Pol III-independent mechanism.

Maf1 binds broadly to the genome and regulates expression of RNA Pol II-transcribed genes involved in retinal proliferation and differentiation

MAF1 has been shown previously to act as a TF to regulate expression of some selective RNA Pol II-transcribed genes.[20,22,30,31] To explore its TF function as a possible Pol III-independent mechanism during retinal development, we performed CUT&Tag assay to identify the genomic sites bound by Maf1 in P7 mouse retinal cells. A total of 8,782 peaks were identified which were highly enriched for two DNA binding motifs: CCAAT and a GC-rich one, as determined by a *de novo* motif search (Figures 7C and 7D). The Maf1 peaks were narrower than but coincided with the peaks of histone H3K27 acetylation (H3K27ac) (Figures 7E and 7F), which is a well-established chromatin marker of active enhancers and promoters, suggesting that Maf1 may indeed act as a broadly functional TF to directly bind to DNA to regulate Pol II gene expression. Consistent with it being a TF, the great majority of Maf1 binding peaks were located in the promoter, intron, and intergenic regions of the genome (Figure 7G).

To examine the functions of Maf1-bound genes, we performed GO and KEGG pathway enrichment analyses. These revealed that the Maf1 peak-associated genes were primarily enriched for those involved in regulation of neurogenesis, forebrain development, axonogenesis, developmental cell growth, cell cycle, regulation of cell growth, Wnt signaling pathway, cAMP signaling pathway, and so on (Figures 7H and 7I), suggesting that *Maf1* may modulate retinal cell proliferation and differentiation by regulating key developmental genes and signaling pathways. Consistent with this idea, Maf1 was seen to bind to the promoter regions of many cell cycle genes such as *Fzr1*, *Stag1*, *Cenpf*, and *Anapc4*, Wnt signaling pathway genes *Axin1*, *Dvl3*, and *Gsk3b*, cAMP signaling pathway genes *Creb1* and *Creb3*, and other retinal

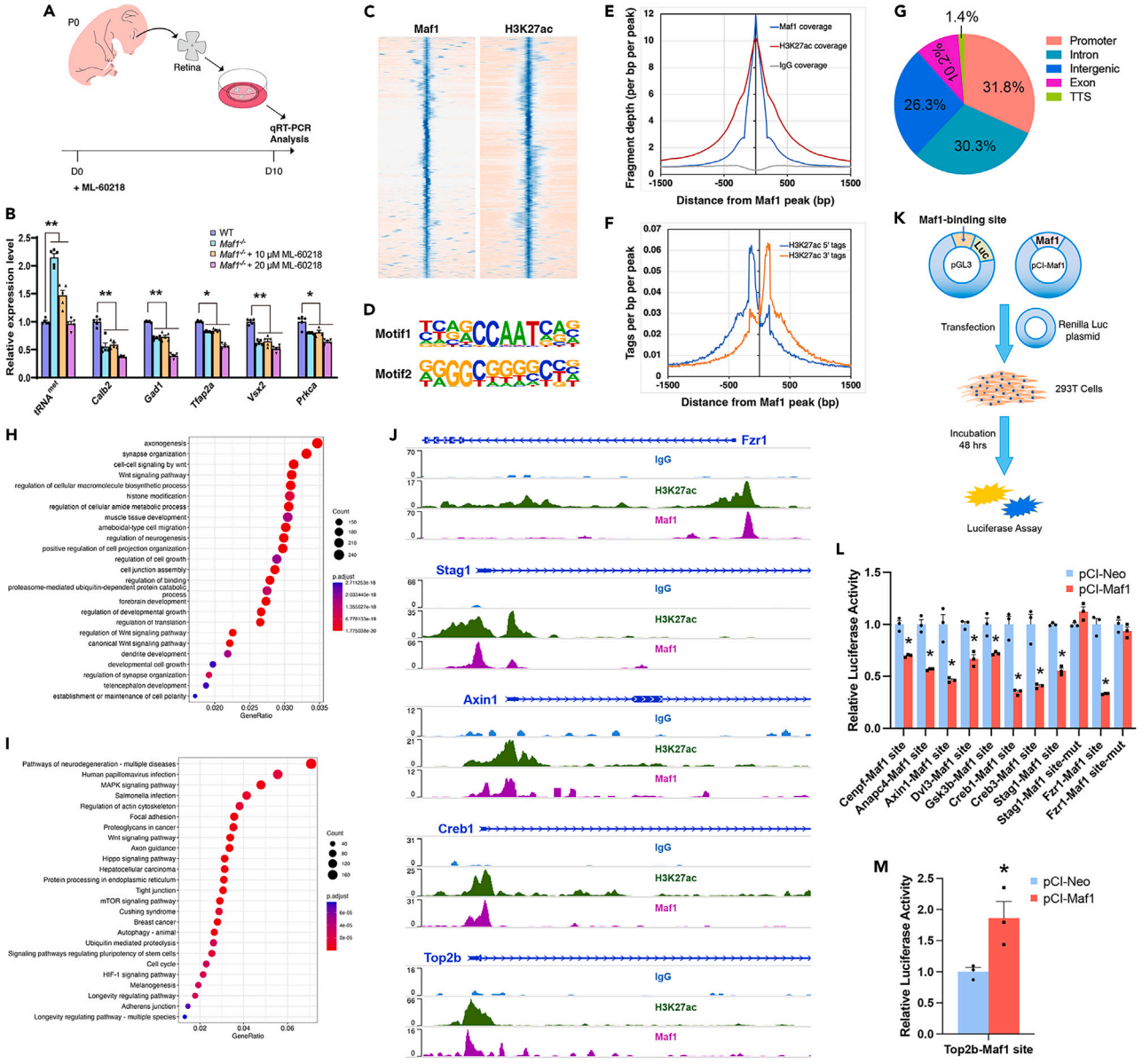

Figure 7. Regulation of retinal cell differentiation and proliferation by *Maf1* via RNA Pol III-independent mechanism

(A) Schematic illustration of *in vitro* culture of P0 retinal explants.

(B) qRT-PCR assay of the RNA expression levels of the indicated cell type-specific marker genes and $tRNA^{Met}$ in WT and $Maf1^{-/-}$ retinal explants as well as in $Maf1^{-/-}$ retinal explants cultured in the presence of 10 or 20 μM ML-60218. Data are presented as mean ± SEM (n = 4 or 5). *p < 0.01, **p < 0.0001.

(C) Heatmaps of Maf1 and H3K27ac CUT&Tag signals in P7 mouse retinal cells within an 8 kb window centered around the peak summit.

(D) The two top-ranked Maf1-binding motifs identified by *de novo* motif search in a 300-bp window centered at the peak summit.

(E) CUT&Tag fragment coverage of Maf1, H3K27ac, and IgG centered around the Maf1 peak summit.

(F) The 5′ and 3′ tags (reads) from the H3K27ac-marked nucleosomes are distributed near the Maf1 peaks.

(G) Frequency of Maf1 peaks located in the promoter, intron, intergenic, exon, and TTS (transcription termination site) regions.

(H and I) GO (H) and KEGG pathway (I) enrichment analyses of Maf1 peak-associated genes.

(J) Genome browser view of Maf1, H3K27ac and IgG CUT&Tag signals at the *Fzr1*, *Stag1*, *Axin1*, *Creb1*, and *Top2b* loci. The y axis represents the number of normalized reads.

(K) Schematic of the luciferase assay. DNA fragments containing Maf1-binding sites identified in various genes were inserted upstream of *Luc* (luciferase) in the pGL3 reporter plasmid.

Figure 7. *Continued*

(L) Relative luciferase activities after cotransfection of the indicated reporter plasmids (Maf1-binding sites or mutant Maf1-binding sites in pGL3-promoter vector) with control (pCI-Neo) or Maf1 (pCI-Maf1) expression plasmids in 293T cells. Histograms represent the mean ± SEM of triplicate assays in a single experiment. *$p < 0.0001$.

(M) Relative luciferase activities after cotransfection of the indicated reporter plasmid (*Top2b* Maf1-binding site in pGL3-basic vector) with control or Maf1 expression plasmids in 293T cells. Histograms represent the mean ± SEM of triplicate assays in a single experiment. *$p < 0.05$.

developmental regulatory genes such as *Top2b* (Figure 7J and S18). All of these genes contained the CCAAT and/or GC-rich motifs in Maf1-bound sequences. To test whether Maf1 was able to regulate expression of these bound genes, we subcloned some of the Maf1-binding sequences into a luciferase reporter plasmid (Figure 7K). In 293T cells, compared to the control, transient transfection of a Maf1 expression plasmid significantly inhibited the luciferase activity of reporter plasmids containing Maf1-binding sites of *Cenpf*, *Anapc4*, *Axin1*, *Dvl3*, *Gsk3b*, *Creb1*, *Creb3*, *Stag1*, *or Fzr1* but increased the luciferase activity of the reporter plasmid containing the *Top2b* Maf1-binding site (Figures 7L and 7M), indicating that Maf1 can indeed act as a TF to activate or repress transcription of Pol II-transcribed genes. The repression activity of Maf1 appeared to depend on the GC-rich and CCAAT motifs because when mutant Maf1-binding sites from *Stag1* or *Fzr1* were used in which these motifs were deleted (Table S4), Maf1 expression did not cause any significant change in luciferase activity (Figure 7L). Since Wnt signaling has been shown to suppress retinal cell differentiation whereas Top2b has the opposite effect,[48–50] and CREB (cAMP responsive element binding protein) signaling is involved in retinal cell proliferation and survival,[51–54] these results suggest that Maf1 may promote retinal neuron differentiation while suppressing retinal cell proliferation by transcriptionally activating *Top2b* expression as well as repressing expression of Wnt and CREB signaling pathway genes.

DISCUSSION

Maf1 controls the generation of retinal neuron cell types by modulating their differentiation

In this work, we have provided multiple lines of evidence to demonstrate that Maf1 is involved in regulating retinal neuron number. First, *in situ* hybridization and immunostaining showed that Maf1 was transiently expressed in most RPCs in the developing retina, suggesting a possibility of its involvement in the generation of all retinal neuron types. Second, at the gross level, OCT and histochemical staining revealed that *Maf1* deletion in mice caused retinal thickness decrease and overall reduction of cell number in all three retinal cellular layers, respectively. These detrimental alterations were consistent with the observed decrease in amplitudes of both a- and b-waves of ERG responses as well as the diminished OPs in *Maf1* null mutant mice. These weakened ERG responses well agree with the idea that optimally functional retinal circuitry may not be formed without the production of appropriate number of retinal neurons. Finally, at the molecular level, qRT-PCR assay and immunolabeling showed that in the *Maf1* null retina, the expression of molecular markers for all 6 neuron types was downregulated and the number of all neuron types was reduced. By contrast, *Maf1* inactivation did not appear to affect the number of Müller cells or their marker gene expression.

During retinogenesis, Maf1 is unlikely involved in the determination of neuron fates because the great majority of cells of all 6 neuron types are present in adult *Maf1* null retinas. Consistent with this conclusion, *Maf1* inactivation caused a deficiency in early differentiation of ganglion, amacrine, horizontal, and photoreceptor cells. In developing null retinas, bulk RNA-seq, scRNA-seq, qRT-PCR, and immunostaining analyses revealed downregulation of various TF genes required for the differentiation of these retinal neuron types, as well as downregulation of molecular markers for all these neuron types at the time of their differentiation. Moreover, although scRNA-seq analysis revealed grossly normal cell lineage trajectories in developing postnatal *Maf1* null retinas, the cell numbers in the terminal clusters and mature cell type clusters were reduced compared to control retinas, indicating that the absence of *Maf1* perturbed differentiation of retinal neuronal lineages from RPCs. Apart from controlling retinal neuron number by regulating cell differentiation, Maf1 may have a more general role in controlling tissue size by a similar mechanism. For example, it has been shown recently that transgenic Maf1 overexpression in mesenchyme caused an increase in bone mass by promoting osteoblast differentiation.[34]

Maf1 negatively regulates RPC proliferation by both RNA Pol III- and Pol II-dependent mechanisms

Our experimental results have demonstrated that Maf1 normally suppresses RPC proliferation during retinal development. Thus, there were increased RPCs in S-phase and/or M-phase in *Maf1*$^{-/-}$ embryonic and postnatal retinas, apparently resulting from shortened cell cycle length, as determined by EdU-pulse labeling, EdU/BrdU dual labeling and pH3 immunostaining. Bulk RNA-seq and scRNA-seq analyses also revealed upregulated expression of various cell cycle marker genes and obvious increase in the number of RPCs in S and G2/M phases. One of the major mechanisms underlying cell number control is regulation of progenitor cell proliferation.[1] For instance, β-catenin controls the size of the cerebral cortex by promoting neural progenitor proliferation while FGF15-Hippo signaling negatively regulates the liver size by inhibiting proliferation of hepatocytes.[55,56] Given the overproduction of RPCs in the developing *Maf1* null retina, we anticipated increased number of mature retinal cells but observed the opposite outcome. This resulted from the apparent degeneration of the extra RPCs by apoptosis, perhaps due to their improper differentiation in the absence of *Maf1*. Therefore, given the observed increase of dividing RPCs, the reduced neuron number in *Maf1* null retinas can be hardly explained by the reduced generation of RPCs during retinogenesis.

RNA Pol III is responsible for the transcription of tRNA, 5S rRNA, and other small RNAs such as U6 RNA, which contribute to protein synthesis required for cell proliferation.[57,58] Therefore, one major mechanism of how Maf1 may inhibit RPC proliferation is by repressing

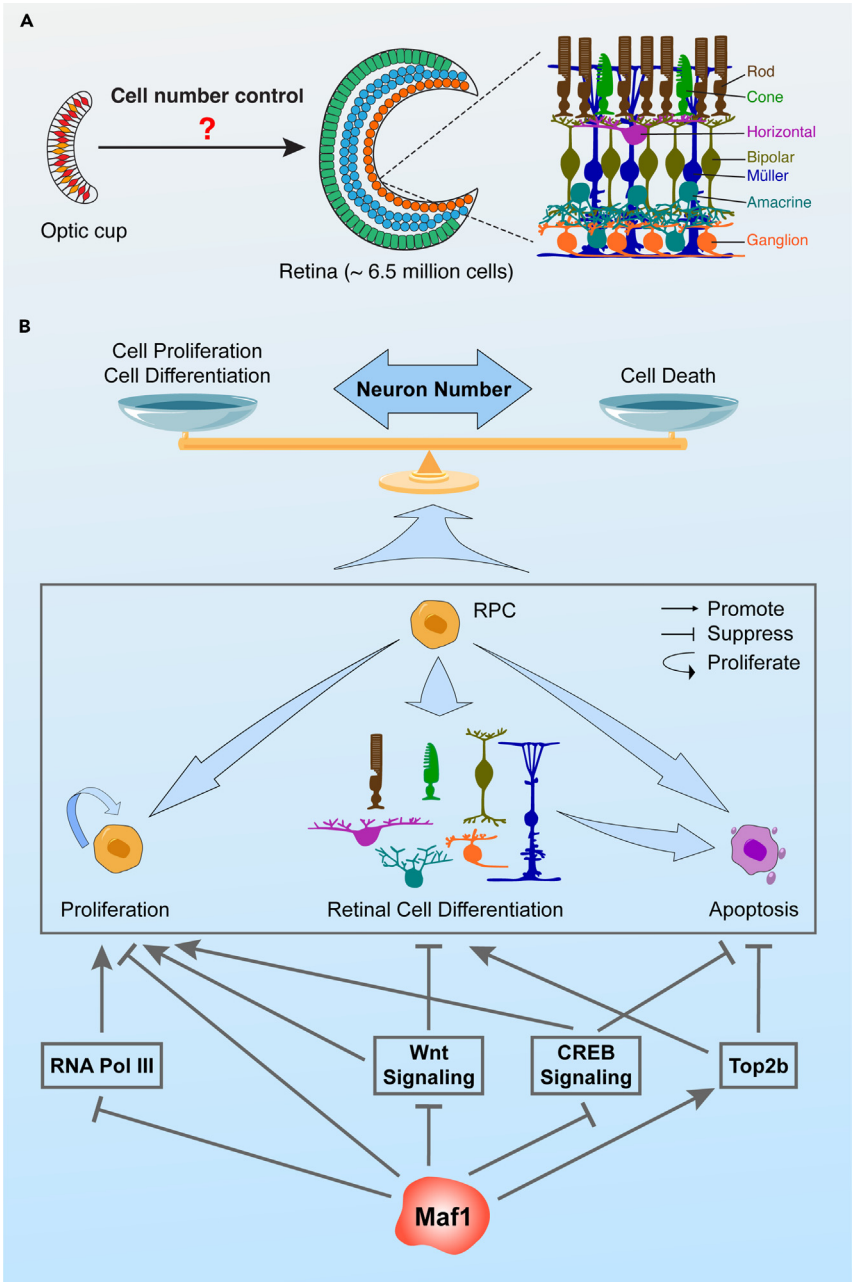

Figure 8. Work model of how Maf1 may control retinal neuron number

(A) During retinogenesis, the 6.5-million-cell murine retina, which is composed of six major neuron types and one glial cell type, is developed from the small optic cup containing multipotent retinal progenitor cells (RPCs). At present, however, the molecular basis underlying the generation of appropriate number of retinal neurons remains unclear.

(B) Maf1 may modulate the generation of correct number of retinal neurons by a balanced regulation of cell proliferation, differentiation, and death via both RNA Pol III-dependent and Pol II-dependent mechanisms. It may negatively regulate RPC proliferation by acting as a major repressor of Pol III as well as by repressing expression of cell cycle genes and genes associated with Wnt and CREB signaling. Meanwhile, it may positively regulate retinal neuron differentiation by repressing expression of Wnt signaling-associated genes and activating Top2b expression. Maf1-regulated Top2b and CREB signaling appear to be also involved in apoptotic cell death during retinogenesis.

RNA Pol III-dependent transcription (Figure 8). This was shown to be the case since *Maf1* inactivation led to great upregulation in expression of *tRNA^{Met}*, *tRNA^{Leu}*, *5S rRNA, and U6 RNA* in the retina. In addition, our chromatin profiling and reporter transcription assay demonstrated that Maf1 not only occupied the promoter regions of many cell cycle genes but was able to repress gene expression through the binding sites.

Moreover, Maf1 similarly bound to and repressed some genes in the Wnt and CREB signaling pathways, which in general promote cell proliferation. Therefore, Maf1 may also inhibit RPC proliferation by suppressing RNA Pol II-dependent transcription (Figure 8).

Maf1 acts as a broadly functional TF to regulate expression of RNA Pol II-transcribed genes

Given that RNA Pol III inhibition failed to rescue neuron differentiation defects in *Maf1* null retinas and that RPCs were overproduced in the mutant, we speculate that Maf1 may control retinal neuron differentiation primarily by an RNA Pol III-independent mechanism. Similarly, Maf1 has recently been implicated in regulating osteoblast differentiation by an RNA Pol III-independent mechanism. Its overexpression promoted osteoblast differentiation whereas its knockdown had the opposite effect, despite the fact that reducing RNA Pol III-dependent transcription inhibited osteoblast differentiation.[34] Interestingly, Maf1 overexpression and direct inhibition of RNA Pol III-dependent transcription led to quite distinct alterations in global gene expression profiles,[34] further indicating an RNA Pol III-independent regulatory mechanism. By contrast, Maf1 has been shown to regulate adipocyte differentiation mainly by suppression of RNA Pol III-dependent transcription,[33,34] suggesting that Maf1 may modulate differentiation via an RNA Pol III-dependent or -independent mechanism depending on tissue types.

We determined the possibility that Maf1 may function as a TF to execute its RNA Pol III-independent function by CUT&Tag chromatin profiling and reporter transcription assay. These analyses have indicated that Maf1 may bind to and regulate many more RNA Pol II-transcribed genes than previously thought. Previous reports have shown that Maf1 is able to bind to and regulate transcription from the promoters of a set of select genes including *TBP*, *Fasn*, *PTEN*, and CREB-associated genes.[20,22,30,31] And one study of genome-wide binding profiles for Maf1 by DamIP-seq detected Maf1 at the promoters of RNA Pol III-transcribed genes but hardly any Maf1 at the promoters of RNA Pol II-transcribed genes.[59] However, our CUT&Tag chromatin profiling in the developing retina yielded thousands of binding peaks, of which the great majority are associated with Pol II-transcribed genes. The Maf1 binding peaks are mostly overlapping with the H3K27ac sites and distributed in the promoter, intron, and intergenic regions of the genome, which are hallmarks of TFs. Indeed, Maf1 was able to repress or activate reporter gene expression through a variety of the binding sites located at the promoters of RNA Pol II-transcribed genes, suggesting that Maf1 may act as a TF to directly bind to DNA and widely regulate Pol II-dependent gene expression.

Maf1 as a transcriptional repressor or activator in regulating expression of cell signaling and developmental genes involved in retinal proliferation and differentiation

Our work has shown that Maf1 functions mainly as a transcriptional repressor for RNA Pol II, just as it is the major repressor of Pol III. Therefore, among 10 tested RNA Pol II-transcribed genes, we found that Maf1 repressed reporter gene expression from its binding sites in 9 of them (Figure 7). In the CUT&Tag chromatin profiling experiment, Wnt signaling and cAMP signaling pathways were among the GO terms and KEGG pathways enriched for the Maf1 peak-associated genes, and reporter transcription assay indeed confirmed the ability for Maf1 to repress the expression of the Wnt signaling pathway genes *Axin1*, *Dvl3*, and *Gsk3b* and the cAMP signaling pathway genes *Creb1* and *Creb3*. Wnt signaling has been demonstrated to play a crucial role in regulating RPC proliferation and differentiation. In developing *Xenopus* and chick retinas, overexpression of Wnt2b or constitutively active β-catenin inhibited neuron differentiation while promoting RPC proliferation and the cell fates of ciliary boy and iris, by downregulating the expression of multiple proneural bHLH genes as well as activating the expression of *Sox2* and *Notch*.[60–62] In contrast, blocking Wnt signaling by knocking down *Xfz5* or *Sox2* resulted in decreased RPC proliferation and increased Müller cell differentiation.[63,64] Similarly, in mouse embryonic eyecups, activation of Wnt signaling by Wnt3a treatment suppressed retinal neurogenesis while promoting the cell fates of the ciliary margin.[65] CREB has been shown to be required for proper formation of the developing mouse retina and for growth and survival of neural progenitors.[51] And in response to cellular signals, it promotes or inhibits the death of developing chick retinal cells both *in vitro* and *in vivo* by phosphorylation/dephosphorylation.[53,54] In addition, activation of CaMKII-CREB signaling effectively protects adult mouse RGCs from injury-induced degeneration.[52] Similarly, Maf1 impedes cortical neural repair in part by suppressing the expression of CREB-associated genes.[31] Thus, Maf1 may promote retinal neuron differentiation and suppress RPC proliferation and retinal cell death by inhibiting the Wnt and CREB signaling pathways (Figure 8). Maf1 knockdown has recently been shown to promote dendritic growth and branching of hippocampal neurons as well as RGC survival and axon regeneration by regulating the PTEN/mTOR signaling pathway.[32,66] Given the ability of Maf1 to repress *Creb* genes and its demonstrated role in neuron survival and repair, it would be interesting to determine whether CREB signaling also contributes to Maf1 knockdown-induced neuron dendritic morphogenesis and regeneration.

Despite the rare incidence of Maf1 as a transcriptional activator,[22] we have shown that it has the ability to activate gene expression from a binding site present in the promoter region of *Top2b*, which encodes topoisomerase IIβ capable of activating transcription through chromatin modification.[67] In general, Top2b plays an essential role in neural development and survival.[67–69] During retinal development, a zebrafish *Top2b* mutant was found to cause lamina-specific targeting defects in the retina and tectum by RGC axons and dendrites.[50] And conditional ablation of murine *Top2b* revealed a pivotal role for this gene in the terminal differentiation and survival of all retinal cell types as well as in the formation of proper laminar structure.[49] By controlling expression of several key TF genes involved in photoreceptor differentiation, Top2b is required for the proper formation of outer segments and synapses of the rod and cone cells.[48] Thus, Maf1 may participate in retinal neuron differentiation and maintenance in part by regulating *Top2b* expression (Figure 8).

In summary, our study has demonstrated that *Maf1* inactivation in mice causes a decrease in retinal thickness and neuron number, which results in attenuated ERG responses. The absence of *Maf1* leads to anomalous differentiation of all retinal neuron types primarily by an RNA

Pol II-dependent mechanism while it promotes RPC proliferation via both Pol III- and Pol II-dependent mechanisms. In spite of the increased RPCs which are subsequently removed by apoptosis in knockout retinas, *Maf1* ablation substantially reduces the generation of retinal neurons during development. As a transcriptional repressor or activator depending on the context, Maf1 binds widely to the genome to regulate the expression of a large set of RNA Pol II-transcribed genes. These include cell cycle genes, Wnt and CREB signaling pathway genes, and *Top2b*, which are involved in retinal cell proliferation, differentiation, and/or survival. Our data together reveal that Maf1 may control the generation of appropriate neuron number during retinogenesis by a balanced regulation of cell proliferation, differentiation, and death via both RNA Pol III-dependent and Pol II-dependent mechanisms (Figure 8).

Limitations of the study

Our findings demonstrate that Maf1 plays an important role in the control of retinal neuron number during mammalian retinogenesis. However, a conventional *Maf1* knockout mouse line was used in this study, making it hard to distinguish indirect effects of *Maf1* inactivation on retinal development, if there are any. It will be necessary to generate tissue-specific and cell type-specific conditional *Maf1* knockout mice to tease out cell type-specific, tissue-specific, and early versus late requirements.

STAR★METHODS

Detailed methods are provided in the online version of this paper and include the following:

- KEY RESOURCES TABLE
- RESOURCE AVAILABILITY
  - Lead contact
  - Materials availability
  - Data and code availability
- EXPERIMENTAL MODEL AND STUDY PARTICIPANT DETAILS
  - Animals
  - Cell culture
- METHOD DETAILS
  - Quantitative real-time PCR (qRT-PCR)
  - Immunohistochemistry
  - Automated Western immunoblotting
  - RNA *in situ* hybridization
  - Optic coherence tomography (OCT) analysis
  - Hematoxylin-eosin (HE) staining and thickness measurement
  - Lens organ culture
  - Electroretinography (ERG)
- RNA-SEQ AND SCRNA-SEQ ANALYSES
  - *In vitro* retinal explant culture
  - CUT&Tag assay
  - Dual-luciferase reporter assays
  - EdU, BrdU and TUNEL labeling
- QUANTIFICATION AND STATISTICAL ANALYSIS

SUPPLEMENTAL INFORMATION

Supplemental information can be found online at https://doi.org/10.1016/j.isci.2023.108544.

ACKNOWLEDGMENTS

We thank Dr. Xintong Zheng and the staff of the Core Facilities of the State Key Laboratory of Ophthalmology, Zhongshan Ophthalmic Center for technical support. This work was supported in part by the National Natural Science Foundation of China (81970794, 32270864, and 81721003), Science and Technology Planning Projects of Guangzhou City (201904020036), "Technology Innovation 2030-Major Projects" on Brain Science and Brain-Like Computing of the Ministry of Science and Technology of China (2021ZD0202603), Local Innovative and Research Teams Project of Guangdong Pearl River Talents Program, the Science and Technology Planning Project of Guangdong Province (2023B1212060018), and the Fundamental Research Funds of the State Key Laboratory of Ophthalmology, Sun Yat-sen University.

AUTHOR CONTRIBUTIONS

M.X. and X.F.S.Z conceived and designed the research. Y.L., D.X., H.C., and M.X. performed the experiments and analyzed the data. M.X. and Y.L. interpreted the data and wrote the manuscript. All authors contributed to critical reading of the manuscript.

DECLARATION OF INTERESTS

The authors declare no competing interests.

INCLUSION AND DIVERSITY

We support inclusive, diverse, and equitable conduct of research.

Received: May 4, 2023
Revised: October 17, 2023
Accepted: November 20, 2023
Published: November 23, 2023

REFERENCES

1. Williams, R.W., and Herrup, K. (1988). The control of neuron number. Annu. Rev. Neurosci. *11*, 423–453.
2. Jeon, C.J., Strettoi, E., and Masland, R.H. (1998). The major cell populations of the mouse retina. J. Neurosci. *18*, 8936–8946.
3. Keeley, P.W., Whitney, I.E., Madsen, N.R., St John, A.J., Borhanian, S., Leong, S.A., Williams, R.W., and Reese, B.E. (2014). Independent genomic control of neuronal number across retinal cell types. Dev. Cell *30*, 103–109.
4. Reese, B.E., and Keeley, P.W. (2016). Genomic control of neuronal demographics in the retina. Prog. Retin. Eye Res. *55*, 246–259.
5. Hamel, C.P. (2007). Cone rod dystrophies. Orphanet J. Rare Dis. *2*, 7.
6. Furukawa, T., Morrow, E.M., Li, T., Davis, F.C., and Cepko, C.L. (1999). Retinopathy and attenuated circadian entrainment in Crx-deficient mice. Nat. Genet. *23*, 466–470.
7. Tsang, S.H., and Sharma, T. (2018). Enhanced S-cone syndrome (Goldmann-Favre syndrome). Adv. Exp. Med. Biol. *1085*, 153–156.
8. Haider, N.B., Jacobson, S.G., Cideciyan, A.V., Swiderski, R., Streb, L.M., Searby, C., Beck, G., Hockey, R., Hanna, D.B., Gorman, S., et al. (2000). Mutation of a nuclear receptor gene, NR2E3, causes enhanced S cone syndrome, a disorder of retinal cell fate. Nat. Genet. *24*, 127–131.
9. Weinreb, R.N., Aung, T., and Medeiros, F.A. (2014). The pathophysiology and treatment of glaucoma: a review. JAMA *311*, 1901–1911.
10. Quigley, H.A. (2011). Glaucoma. Lancet *377*, 1367–1377.
11. Strom, R.C., and Williams, R.W. (1998). Cell production and cell death in the generation of variation in neuron number. J. Neurosci. *18*, 9948–9953.
12. Young, R.W. (1985). Cell differentiation in the retina of the mouse. Anat. Rec. *212*, 199–205.
13. Cepko, C. (2014). Intrinsically different retinal progenitor cells produce specific types of progeny. Nat. Rev. Neurosci. *15*, 615–627.
14. Livesey, F.J., and Cepko, C.L. (2001). Vertebrate neural cell-fate determination: lessons from the retina. Nat. Rev. Neurosci. *2*, 109–118.
15. Xiang, M. (2013). Intrinsic control of mammalian retinogenesis. Cell. Mol. Life Sci. *70*, 2519–2532.
16. Hatakeyama, J., and Kageyama, R. (2004). Retinal cell fate determination and bHLH factors. Semin. Cell Dev. Biol. *15*, 83–89.
17. Agathocleous, M., and Harris, W.A. (2009). From progenitors to differentiated cells in the vertebrate retina. Annu. Rev. Cell Dev. Biol. *25*, 45–69.
18. Willis, I.M., and Moir, R.D. (2018). Signaling to and from the RNA Polymerase III transcription and processing machinery. In Annual Review of Biochemistry, R.D. Kornberg, ed., pp. 75–100.
19. Hammerquist, A.M., Escorcia, W., and Curran, S.P. (2021). Maf1 regulates intracellular lipid homeostasis in response to DNA damage response activation. Mol. Biol. Cell *32*, 1086–1093.
20. Palian, B.M., Rohira, A.D., Johnson, S.A.S., He, L., Zheng, N., Dubeau, L., Stiles, B.L., and Johnson, D.L. (2014). Maf1 Is a novel target of PTEN and PI3K signaling that negatively regulates oncogenesis and lipid metabolism. PLoS Genet. *10*, e1004789.
21. Johnson, D.L., and Stiles, B.L. (2016). Maf1, A New PTEN Target Linking RNA and Lipid Metabolism. Trends Endocrinol. Metab. *27*, 742–750.
22. Li, Y., Tsang, C.K., Wang, S., Li, X.X., Yang, Y., Fu, L., Huang, W., Li, M., Wang, H.Y., and Zheng, X.F.S. (2016). MAF1 suppresses AKT-mTOR signaling and liver cancer through activation of PTEN transcription. Hepatology *63*, 1928–1942.
23. Marshall, L., and White, R.J. (2008). Non-coding RNA production by RNA polymerase III is implicated in cancer. Nat. Rev. Cancer *8*, 911–914.
24. Hokonohara, K., Nishida, N., Miyoshi, N., Takahashi, H., Haraguchi, N., Hata, T., Matsuda, C., Mizushima, T., Doki, Y., and Mori, M. (2019). Involvement of MAF1 homolog, negative regulator of RNA polymerase III in colorectal cancer progression. Int. J. Oncol. *54*, 1001–1009.
25. Zhang, S., Li, X., Wang, H.Y., and Steven Zheng, X.F. (2018). Beyond regulation of pol III: Role of MAF1 in growth, metabolism, aging and cancer. Biochim. Biophys. Acta. Gene Regul. Mech. *1861*, 338–343.
26. Noguchi, C., Wang, L., Shetty, M., Mell, J.C., Sell, C., and Noguchi, E. (2021). Maf1 limits RNA polymerase III-directed transcription to preserve genomic integrity and extend lifespan. Cell Cycle *20*, 247–255.
27. Shetty, M., Noguchi, C., Wilson, S., Martinez, E., Shiozaki, K., Sell, C., Mell, J.C., and Noguchi, E. (2020). Maf1-dependent transcriptional regulation of tRNAs prevents genomic instability and is associated with extended lifespan. Aging Cell *19*, e13068.
28. Graczyk, D., Cieśla, M., and Boguta, M. (2018). Regulation of tRNA synthesis by the general transcription factors of RNA polymerase III - TFIIIB and TFIIIC, and by the MAF1 protein. Biochim. Biophys. Acta. Gene Regul. Mech. *1861*, 320–329.
29. Turowski, T.W., Karkusiewicz, I., Kowal, J., and Boguta, M. (2012). Maf1-mediated repression of RNA polymerase III transcription inhibits tRNA degradation via RTD pathway. RNA *18*, 1823–1832.
30. Johnson, S.S., Zhang, C., Fromm, J., Willis, I.M., and Johnson, D.L. (2007). Mammalian Maf1 is a negative regulator of transcription by all three nuclear RNA polymerases. Mol. Cell *26*, 367–379.
31. Tsang, C.K., Mi, Q., Su, G., Hwa Lee, G., Xie, X., D'Arcangelo, G., Huang, L., and Steven Zheng, X.F. (2023). Maf1 is an intrinsic suppressor against spontaneous neural repair and functional recovery after ischemic stroke. J. Adv. Res. *51*, 73–90.
32. Chen, K., Zhu, L., Guo, L., Pan, Y.B., and Feng, D.F. (2020). Maf1 regulates dendritic morphogenesis and influences learning and memory. Cell Death Dis. *11*, 606.
33. Chen, C.-Y., Lanz, R.B., Walkey, C.J., Chang, W.-H., Lu, W., and Johnson, D.L. (2018). Maf1 and repression of RNA polymerase III-mediated transcription drive adipocyte differentiation. Cell Rep. *24*, 1852–1864.
34. Phillips, E., Ahmad, N., Sun, L., Iben, J., Walkey, C.J., Rusin, A., Yuen, T., Rosen, C.J., Willis, I.M., Zaidi, M., and Johnson, D.L. (2022). MAF1, a repressor of RNA polymerase III-dependent transcription, regulates bone mass. Elife *11*, e74740.
35. Creel, D.J. (2019). Electroretinograms. In Clinical Neurophysiology: Basis and Technical Aspects, pp. 481–493.
36. Wachtmeister, L. (1998). Oscillatory potentials in the retina: what do they reveal. Prog. Retin. Eye Res. *17*, 485–521.
37. Polli, L., Schwan, R., Albuisson, E., Malbos, L., Angioi-Duprez, K., Laprevote, V., and Schwitzer, T. (2021). Oscillatory potentials abnormalities in regular cannabis users: Amacrine cells dysfunction as a marker of central dopaminergic modulation. Prog. Neuro-Psychopharmacol. Biol. Psychiatry *108*, 110083.
38. Dräger, U.C., and Olsen, J.F. (1981). Ganglion cell distribution in the retina of the mouse. Invest. Ophthalmol. Vis. Sci. *20*, 285–293.
39. Ortín-Martínez, A., Nadal-Nicolás, F.M., Jiménez-López, M., Alburquerque-Béjar, J.J., Nieto-López, L., García-Ayuso, D., Villegas-Pérez, M.P., Vidal-Sanz, M., and Agudo-Barriuso, M. (2014). Number and distribution of mouse retinal cone photoreceptors: differences between an albino (Swiss) and a pigmented (C57/BL6) strain. PLoS One *9*, e102392.

40. Salinas-Navarro, M., Mayor-Torroglosa, S., Jiménez-López, M., Avilés-Trigueros, M., Holmes, T.M., Lund, R.D., Villegas-Pérez, M.P., and Vidal-Sanz, M. (2009). A computerized analysis of the entire retinal ganglion cell population and its spatial distribution in adult rats. Vision Res. *49*, 115–126.
41. Camerino, M.J., Engerbretson, I.J., Fife, P.A., Reynolds, N.B., Berria, M.H., Doyle, J.R., Clemons, M.R., Gencarella, M.D., Borghuis, B.G., and Fuerst, P.G. (2021). OFF bipolar cell density varies by subtype, eccentricity, and along the dorsal ventral axis in the mouse retina. J. Comp. Neurol. *529*, 1911–1925.
42. Wu, F., Bard, J.E., Kann, J., Yergeau, D., Sapkota, D., Ge, Y., Hu, Z., Wang, J., Liu, T., and Mu, X. (2021). Single cell transcriptomics reveals lineage trajectory of retinal ganglion cells in wild-type and Atoh7-null retinas. Nat. Commun. *12*, 1465.
43. Stuart, T., Butler, A., Hoffman, P., Hafemeister, C., Papalexi, E., Mauck, W.M., 3rd, Hao, Y., Stoeckius, M., Smibert, P., and Satija, R. (2019). Comprehensive integration of single-cell data. Cell *177*, 1888–1902.e21.
44. Nestorowa, S., Hamey, F.K., Pijuan Sala, B., Diamanti, E., Shepherd, M., Laurenti, E., Wilson, N.K., Kent, D.G., and Göttgens, B. (2016). A single-cell resolution map of mouse hematopoietic stem and progenitor cell differentiation. Blood *128*, e20–e31.
45. Harris, L., Zalucki, O., and Piper, M. (2018). BrdU/EdU dual labeling to determine the cell-cycle dynamics of defined cellular subpopulations. J. Mol. Histol. *49*, 229–234.
46. Martynoga, B., Morrison, H., Price, D.J., and Mason, J.O. (2005). Foxg1 is required for specification of ventral telencephalon and region-specific regulation of dorsal telencephalic precursor proliferation and apoptosis. Dev. Biol. *283*, 113–127.
47. Das, G., Choi, Y., Sicinski, P., and Levine, E.M. (2009). Cyclin D1 fine-tunes the neurogenic output of embryonic retinal progenitor cells. Neural Dev. *4*, 15.
48. Li, Y., Hao, H., Swerdel, M.R., Cho, H.Y., Lee, K.B., Hart, R.P., Lyu, Y.L., and Cai, L. (2017). Top2b is involved in the formation of outer segment and synapse during late-stage photoreceptor differentiation by controlling key genes of photoreceptor transcriptional regulatory network. J. Neurosci. Res. *95*, 1951–1964.
49. Li, Y., Hao, H., Tzatzalos, E., Lin, R.K., Doh, S., Liu, L.F., Lyu, Y.L., and Cai, L. (2014). Topoisomerase IIbeta is required for proper retinal development and survival of postmitotic cells. Biol. Open *3*, 172–184.
50. Nevin, L.M., Xiao, T., Staub, W., and Baier, H. (2011). Topoisomerase IIbeta is required for lamina-specific targeting of retinal ganglion cell axons and dendrites. Development *138*, 2457–2465.
51. Dworkin, S., Malaterre, J., Hollande, F., Darcy, P.K., Ramsay, R.G., and Mantamadiotis, T. (2009). cAMP response element binding protein is required for mouse neural progenitor cell survival and expansion. Stem Cell. *27*, 1347–1357.
52. Guo, X., Zhou, J., Starr, C., Mohns, E.J., Li, Y., Chen, E.P., Yoon, Y., Kellner, C.P., Tanaka, K., Wang, H., et al. (2021). Preservation of vision after CaMKII-mediated protection of retinal ganglion cells. Cell *184*, 4299–4314.e12.
53. Socodato, R., Brito, R., Calaza, K.C., and Paes-de-Carvalho, R. (2011). Developmental regulation of neuronal survival by adenosine in the in vitro and in vivo avian retina depends on a shift of signaling pathways leading to CREB phosphorylation or dephosphorylation. J. Neurochem. *116*, 227–239.
54. Socodato, R., Brito, R., Portugal, C.C., de Oliveira, N.A., Calaza, K.C., and Paes-de-Carvalho, R. (2014). The nitric oxide-cGKII system relays death and survival signals during embryonic retinal development via AKT-induced CREB1 activation. Cell Death Differ. *21*, 915–928.
55. Chenn, A., and Walsh, C.A. (2002). Regulation of cerebral cortical size by control of cell cycle exit in neural precursors. Science *297*, 365–369.
56. Ji, S., Liu, Q., Zhang, S., Chen, Q., Wang, C., Zhang, W., Xiao, C., Li, Y., Nian, C., Li, J., et al. (2019). FGF15 activates Hippo signaling to suppress bile acid metabolism and liver tumorigenesis. Dev. Cell *48*, 460–474.e9.
57. Brooks, R.F. (1977). Continuous protein synthesis is required to maintain the probability of entry into S phase. Cell *12*, 311–317.
58. Marshall, L., Kenneth, N.S., and White, R.J. (2008). Elevated $tRNA_i^{Met}$ synthesis can drive cell proliferation and oncogenic transformation. Cell *133*, 78–89.
59. Orioli, A., Praz, V., Lhôte, P., and Hernandez, N. (2016). Human MAF1 targets and represses active RNA polymerase III genes by preventing recruitment rather than inducing long-term transcriptional arrest. Genome Res. *26*, 624–635.
60. Kubo, F., Takeichi, M., and Nakagawa, S. (2003). Wnt2b controls retinal cell differentiation at the ciliary marginal zone. Development *130*, 587–598.
61. Kubo, F., Takeichi, M., and Nakagawa, S. (2005). Wnt2b inhibits differentiation of retinal progenitor cells in the absence of Notch activity by downregulating the expression of proneural genes. Development *132*, 2759–2770.
62. Cho, S.H., and Cepko, C.L. (2006). Wnt2b/beta-catenin-mediated canonical Wnt signaling determines the peripheral fates of the chick eye. Development *133*, 3167–3177.
63. Van Raay, T.J., Moore, K.B., Iordanova, I., Steele, M., Jamrich, M., Harris, W.A., and Vetter, M.L. (2005). Frizzled 5 signaling governs the neural potential of progenitors in the developing Xenopus retina. Neuron *46*, 23–36.
64. Agathocleous, M., Iordanova, I., Willardsen, M.I., Xue, X.Y., Vetter, M.L., Harris, W.A., and Moore, K.B. (2009). A directional Wnt/beta-catenin-Sox2-proneural pathway regulates the transition from proliferation to differentiation in the Xenopus retina. Development *136*, 3289–3299.
65. Diacou, R., Zhao, Y., Zheng, D., Cvekl, A., and Liu, W. (2018). Six3 and Six6 are jointly required for the maintenance of multipotent retinal progenitors through both positive and negative regulation. Cell Rep. *25*, 2510–2523.e4.
66. Chen, D., Sun, Y.Y., Zhou, L.Y., Yang, S., Hong, F.Y., Liu, X.D., Sun, Z.L., Huang, J., and Feng, D.F. (2022). Maf1 regulates axonal regeneration of retinal ganglion cells after injury. Exp. Neurol. *348*, 113948.
67. Tiwari, V.K., Burger, L., Nikoletopoulou, V., Deogracias, R., Thakurela, S., Wirbelauer, C., Kaut, J., Terranova, R., Hoerner, L., Mielke, C., et al. (2012). Target genes of Topoisomerase IIbeta regulate neuronal survival and are defined by their chromatin state. Proc. Natl. Acad. Sci. USA *109*, E934–E943.
68. Lyu, Y.L., and Wang, J.C. (2003). Aberrant lamination in the cerebral cortex of mouse embryos lacking DNA topoisomerase IIbeta. Proc. Natl. Acad. Sci. USA *100*, 7123–7128.
69. Yang, X., Li, W., Prescott, E.D., Burden, S.J., and Wang, J.C. (2000). DNA topoisomerase IIbeta and neural development. Science *287*, 131–134.
70. Wolock, S.L., Lopez, R., and Klein, A.M. (2019). Scrublet: Computational Identification of Cell Doublets in Single-Cell Transcriptomic Data. Cell Syst. *8*, 281–291.e9.
71. Xiao, D., Deng, Q., Guo, Y., Huang, X., Zou, M., Zhong, J., Rao, P., Xu, Z., Liu, Y., Hu, Y., et al. (2020). Generation of self-organized sensory ganglion organoids and retinal ganglion cells from fibroblasts. Sci. Adv. *6*, eaaz5858.
72. Qiu, X., Mao, Q., Tang, Y., Wang, L., Chawla, R., Pliner, H.A., and Trapnell, C. (2017). Reversed graph embedding resolves complex single-cell trajectories. Nat. Methods *14*, 979–982.
73. Kim, D., Langmead, B., and Salzberg, S.L. (2015). HISAT: a fast spliced aligner with low memory requirements. Nat. Methods *12*, 357–360.
74. Li, S., Mo, Z., Yang, X., Price, S.M., Shen, M.M., and Xiang, M. (2004). Foxn4 controls the genesis of amacrine and horizontal cells by retinal progenitors. Neuron *43*, 795–807.
75. Mo, Z., Li, S., Yang, X., and Xiang, M. (2004). Role of the Barhl2 homeobox gene in the specification of glycinergic amacrine cells. Development *131*, 1607–1618.
76. Dahl, J.A., Jung, I., Aanes, H., Greggains, G.D., Manaf, A., Lerdrup, M., Li, G., Kuan, S., Li, B., Lee, A.Y., et al. (2016). Broad histone H3K4me3 domains in mouse oocytes modulate maternal-to-zygotic transition. Nature *537*, 548–552.
77. Sciavolino, P.J., Abrams, E.W., Yang, L., Austenberg, L.P., Shen, M.M., and Abate-Shen, C. (1997). Tissue-specific expression of murine Nkx3.1 in the male urogenital system. Dev. Dyn. *209*, 127–138.
78. Li, W.C., Kuszak, J.R., Dunn, K., Wang, R.R., Ma, W., Wang, G.M., Spector, A., Leib, M., Cotliar, A.M., Weiss, M., et al. (1995). Lens epithelial cell apoptosis appears to be a common cellular basis for non-congenital cataract development in humans and animals. J. Cell Biol. *130*, 169–181.
79. Wei, W., Liu, B., Jiang, H., Jin, K., and Xiang, M. (2019). Requirement of the Mowat-Wilson syndrome gene Zeb2 in the differentiation and maintenance of non-photoreceptor cell types during retinal development. Mol. Neurobiol. *56*, 1719–1736.
80. Xiao, D., Liu, X., Zhang, M., Zou, M., Deng, Q., Sun, D., Bian, X., Cai, Y., Guo, Y., Liu, S., et al. (2018). Direct reprogramming of fibroblasts into neural stem cells by single non-neural progenitor transcription factor Ptf1a. Nat. Commun. *9*, 2865.
81. Wu, T., Hu, E., Xu, S., Chen, M., Guo, P., Dai, Z., Feng, T., Zhou, L., Tang, W., Zhan, L., et al. (2021). clusterProfiler 4.0: A universal enrichment tool for interpreting omics data. Innovation *2*, 100141.
82. Jin, K., and Xiang, M. (2012). In vitro explant culture and related protocols for the study of mouse retinal development. Methods Mol. Biol. *884*, 155–165.
83. Kaya-Okur, H.S., Wu, S.J., Codomo, C.A., Pledger, E.S., Bryson, T.D., Henikoff, J.G., Ahmad, K., and Henikoff, S. (2019). CUT&Tag for efficient epigenomic profiling of small samples and single cells. Nat. Commun. *10*, 1930.
84. Heinz, S., Benner, C., Spann, N., Bertolino, E., Lin, Y.C., Laslo, P., Cheng, J.X., Murre, C.,

Singh, H., and Glass, C.K. (2010). Simple combinations of lineage-determining transcription factors prime cis-regulatory elements required for macrophage and B cell identities. Mol. Cell *38*, 576–589.

85. Liu, W., Khare, S.L., Liang, X., Peters, M.A., Liu, X., Cepko, C.L., and Xiang, M. (2000). All Brn3 genes can promote retinal ganglion cell differentiation in the chick. Development *127*, 3237–3247.

86. Luo, H., Jin, K., Xie, Z., Qiu, F., Li, S., Zou, M., Cai, L., Hozumi, K., Shima, D.T., and Xiang, M. (2012). Forkhead box N4 (Foxn4) activates Dll4-Notch signaling to suppress photoreceptor cell fates of early retinal progenitors. Proc. Natl. Acad. Sci. USA *109*, E553–E562.

87. Mead, T.J., and Lefebvre, V. (2014). Proliferation assays (BrdU and EdU) on skeletal tissue sections. Methods Mol. Biol. *1130*, 233–243.

STAR★METHODS

KEY RESOURCES TABLE

REAGENT or RESOURCE	SOURCE	IDENTIFIER
Antibodies		
Maf1	GeneTex	Cat# GTX106776; RRID: AB_1950848
Brn3a (Pou4f1)	Millipore	Cat# MAB1585; RRID: AB_94166
Brn3b (Pou4f2)	Santa Cruz Biotech	Cat# sc-6026; RRID: AB_673441
Rbpms	Novus Biologicals	Cat# NBP2-20112; RRID: AB_3075531
Bhlhb5/BETA3 (Bhlhe22)	Santa Cruz Biotech	Cat# sc-6045; RRID: AB_2065343
Calbindin D-28k (Calb1)	Swant	Cat# CB38; RRID: AB_10000340
Chx10 (Vsx2)	Santa Cruz Biotech	Cat# sc-21690; RRID: AB_2216006
GAD65 (Gad2)	BD Biosciences	Cat# 559931; RRID: AB_397380
GAD67 (Gad1)	Millipore	Cat# MAB5406; RRID: AB_2278725
Glutamine synthetase (Glul)	Millipore	Cat# MAB302; RRID: AB_2110656
Sox2	Santa Cruz Biotech	Cat# sc-17320; RRID: AB_2286684
tdTomato	Sicgen	Cat# AB8181-200; RRID: AB_2722750
RFP (tdTomato)	Rockland	Cat# 600-401-379; RRID: AB_2209751
GLYT1 (Slc6a9)	Millipore	Cat# AB1770; RRID: AB_90893
Lim1/2 (Lhx1/2)	Developmental Studies Hybridoma Bank	Cat# 4F2; RRID: AB_531784
Pax6	Millipore	Cat# AB2237; RRID: AB_1587367
Pax6	Developmental Studies Hybridoma Bank	Cat# pax6; RRID: AB_528427
Recoverin (Rcvrn)	Millipore	Cat# AB5585; RRID: AB_2253622
Sox9	Millipore	Cat# AB5535; RRID: AB_2239761
Calretinin (Calb2)	Millipore	Cat# AB1550; RRID: AB_90764
Tfap2a	Abcam	Cat# ab11828; RRID: AB_298610
Cone arrestin (Arr3)	Millipore	Cat# AB15282; RRID: AB_1163387
Protein kinase Cα (Prkca)	Sigma	Cat# P4334; RRID: AB_477345
Phospho-histone H3 (Ser10) (pH3)	Millipore	Cat# 06-570; RRID: AB_310177
β -Tubulin	Abcam	Cat# ab179513; RRID: AB_3073861
BrdU	Thermo Fisher Scientific	Cat# B35128; RRID: AB_2536432
Ki67	Thermo Fisher Scientific	Cat# MA5-14520; RRID: AB_10979488
Alexa Fluor 488 Donkey Anti-Mouse IgG (H+L)	Thermo Fisher Scientific	Cat# A21202; RRID: AB_141607
Alexa Fluor 594 Donkey Anti-Mouse IgG (H+L)	Thermo Fisher Scientific	Cat# A21203; RRID: AB_141633
Alexa Fluor 488 Donkey Anti-Rabbit IgG (H+L)	Thermo Fisher Scientific	Cat# A21206; RRID: AB_2535792
Alexa Fluor 594 Donkey Anti-Rabbit IgG (H+L)	Thermo Fisher Scientific	Cat# A21207; RRID: AB_141637
Alexa Fluor 488 Donkey anti-Goat IgG (H+L)	Thermo Fisher Scientific	Cat# A11055; RRID: AB_2534102
Alexa Fluor 594 Donkey anti-Goat IgG (H+L)	Thermo Fisher Scientific	Cat# A11058; RRID: AB_2534105
Chemicals, peptides, and recombinant proteins		
ML-60218	MedChemExpress	Cat# HY-122122
BrdU	Merck	Cat# B5002
DMEM/F12+GlutaMAX-I	Gibco	Cat# 10565-018
N-2 Supplement (100X)	Gibco	Cat# 17502048
Taurine	Sigma	Cat# T0265-10G
Retinoic acid	Sigma	Cat# R2625

(*Continued on next page*)

Continued

REAGENT or RESOURCE	SOURCE	IDENTIFIER
Normal Donkey Serum	Jackson ImmunoResearch Labs	Cat# 017-000-121
Critical commercial assays		
Click-iT™ Plus EdU Alexa Fluor™ 555Imaging Kit	Thermo Fishers	Cat# C10638
eBioscience™ BrdU Kit for IHC/ICC Immunofluorescence eFluor™ 660	Thermo Fishers	Cat# 8850-6599-45
In Situ Cell Death Detection Kit	Roche	Cat# 11684795910
CUT&Tag-IT™ Assay Kit	Active Motif	Cat# 53160
Deposited data		
RNA-seq data	NCBI	Sequence Read Archive (SRA) accession code: PRJNA978356 (https://www.ncbi.nlm.nih.gov/sra/PRJNA978356)
scRNA-seq data	NCBI	Sequence Read Archive (SRA) accession code: PRJNA987385 (https://www.ncbi.nlm.nih.gov/sra/PRJNA987385)
CUT&Tag data	NCBI	Sequence Read Archive (SRA) accession code: PRJNA993370 (https://www.ncbi.nlm.nih.gov/sra/PRJNA993370)
Experimental models: Organisms/strains		
Maf1 knockout mouse line	This paper	N/A
Oligonucleotides		
Primers for qRT-PCR, see Table S1	This paper	N/A
Maf1 mutant binding sites, see Table S2	This paper	N/A
Recombinant DNA		
pGL3-promoter	Promega	Cat# E1761
pGL3-basic	Promega	Cat# E1751
pCI-neo	YouBio	Cat# VT1071
pRL-TK	Promega	Cat# E2241
pCI-Maf1	This paper	N/A
pGL3-Cenpf-promoter	This paper	N/A
pGL3-Fzr1-promoter	This paper	N/A
pGL3-Anapc4-promoter	This paper	N/A
pGL3-Stag1-promoter	This paper	N/A
pGL3-Axin1-promoter	This paper	N/A
pGL3-Dvl3-promoter	This paper	N/A
pGL3-Gsk3b-promoter	This paper	N/A
pGL3-Creb1-promoter	This paper	N/A
pGL3-Creb3-promoter	This paper	N/A
pGL3-Top2b-basic	This paper	N/A
Software and algorithms		
ImageJ	NIH	https://imagej.nih.gov/ij/
ZEN 2.0 (blue edition)	Carl Zeiss	https://www.zeiss.com/microscopy/int/products/microscope-software.html
GraphPad Prism 8.0	GraphPad	https://www.graphpad.com/

(*Continued on next page*)

Continued

REAGENT or RESOURCE	SOURCE	IDENTIFIER
RStudio	R Core Team	https://cran.r-project.org/
Seurat 4	Satija lab	https://satijalab.org/seurat/index.html
Monocle 3	Qiu, Xiaojie et al.[70]	https://cole-trapnell-lab.github.io/monocle3/
Scrublet	Wolock, Samuel L et al.[71]	https://github.com/AllonKleinLab/scrublet
ClusterProfiler	Wu, Tianzhi et al.[72]	https://bioconductor.org/packages/release/bioc/html/clusterProfiler.html
HOMER (Hypergeometric Optimization of Motif EnRichment)	Heinz, Sven et al.[73]	http://homer.ucsd.edu/homer/index.html
Compass for SW	ProteinSimple	https://www.bio-techne.com/resources/instrument-software-download-center/compass-software-simple-western

RESOURCE AVAILABILITY

Lead contact

Further information and requests for resources and reagents should be directed to and will be fulfilled by the lead contact, Mengqing Xiang (xiangmq3@mail.sysu.edu.cn).

Materials availability

Materials generated in this study are available from the lead contact's laboratory upon request.

Data and code availability

- RNA-seq data (https://www.ncbi.nlm.nih.gov/sra/PRJNA978356), scRNA-seq data (https://www.ncbi.nlm.nih.gov/sra/PRJNA987385) and CUT&Tag data (https://www.ncbi.nlm.nih.gov/sra/PRJNA993370) have been deposited at NCBI and are publicly available as of the date of publication. Accession numbers are listed in the key resources table.
- This paper does not report original code.
- Any additional information required to reanalyze the data reported in this paper is available from the lead contact upon request.

EXPERIMENTAL MODEL AND STUDY PARTICIPANT DETAILS

Animals

The *Maf1* knockout mouse line was generated by Shanghai Model Organisms Center, Inc. (Shanghai, China) using the CRISPR/Cas9 gene-editing technology on a C57BL/6 genetic background (Figure S3A). All experiments involved with *Maf1* mutant mice were performed using animals of F4-F7 generations. For mouse genotyping, we concurrently used three primers (F1, F2 and R1) to distinguish the *Maf1* WT and mutant alleles, and the following PCR protocol was used: 95°C for 5 min, followed by 35 cycles of 95°C for 30 s, 58°C for 30 s, and 72°C for 30 s, and then a final extension at 72°C for 5 min. Whereas the paired primers F1 and R1 produced a 409-bp fragment from the WT allele, the paired primers F2 and R1 yielded a 327-bp fragment from the mutant allele. The primer sequences are following: Forward primer 1 (F1): 5'-GTAAGATGGCGGGAGATGATAAAC-3'; Forward primer 2 (F2): 5'-CTGGGGGCCGAGAGCAAGTAAAAT-3'; and Reverse primer 1 (R1): 5'-CAAGTGGGGATGGCAATGAGA-3'. The C57BL/6 mice were purchased from the Vital River Laboratories (Beijing, China). The starting stage of mouse embryos was defined by taking the morning as E0.5 when the copulation plug was seen. All genotypes were determined by PCR.

For Maf1 expression pattern assay, E12.5, E14.5, E16.5, E18.5, P0, P4, P8, and P21 C57BL/6 mice were used for RNA in situ hybridization and immunostaining analysis. For tdTomato immunostaining analysis, E12.5, E14.5, E16.5, E18.5, P0, P4, P8, P12 and 1 month $Maf1^{+/-}$ mice were used. For retinal thickness analysis, 1-month $Maf1^{+/+}$ and $Maf1^{-/-}$ mice were used for OCT and HE staining. For ERG analysis, 2-month and 6-month $Maf1^{+/+}$ and $Maf1^{-/-}$ mice were used. For lens organ culture, 1-month control and $Maf1^{-/-}$ mice were used. For comparative immunostaining assays, $Maf1^{+/+}$ mice at P0, P4, P6, P7, P8, P9, P11, P12, and 1-month, $Maf1^{+/-}$ mice at E12.5, E14.5, E16.5, and E18.5, and $Maf1^{-/-}$ mice at E12.5, E14.5, E16.5, E18.5, P0, P4, P 6, P7, P8, P9, P11, P12, and 1-month were used. For EdU, BrdU and TUNEL labeling, $Maf1^{+/+}$ mice at E14, $Maf1^{+/-}$ mice at E18.5, and $Maf1^{-/-}$ mice at E14 and E18.5 were used. For retinal explant culture, P0 $Maf1^{+/+}$ and $Maf1^{-/-}$ mice were used. For RNA-seq analysis, P0 and P8 $Maf1^{+/+}$ and $Maf1^{-/-}$ mice were used. For scRNA-seq analysis, P3 and P7 $Maf1^{+/+}$ and $Maf1^{-/-}$ mice were used. For CUT&Tag assay, P7 C57BL/6 mice were used.

Both male and female mice were used. All mice were bred and raised in SPF-level animal rooms. All experiments on mice were performed according to the IACUC (Institutional Animal Care and Use Committee) standards, and approved by Zhongshan Ophthalmic Center, Sun Yat-sen University.

Cell culture

HEK293T cells (ATCC, CRL-3216), which were purchased from ATCC, were cultured and expanded in the MEF (mouse embryonic fibroblast) medium [Dulbecco's modified Eagle's medium (DMEM)/High Glucose (HyClone), 10% fetal bovine serum (Gibco), 1% penicillin/streptomycin (Gibco), and 1% MEM nonessential amino acids (NEAA) (Gibco)]. They were tested for mycoplasma contamination before experiments.

METHOD DETAILS

Quantitative real-time PCR (qRT-PCR)

The TRIzol reagent (Invitrogen) was used to isolate total RNA of retinas from P0, P8 and one-month-old control and *Maf1*$^{-/-}$ mice as well as total RNA of cultured retinal explants. RNA (1 μg) from each sample of different genotypes was converted to cDNA using the HiScript III RT SuperMix for qPCR (+gDNA wiper) (Vazyme). qRT-PCR was then performed using the SYBR fast qPCR master mix (Kapa) in the Light Cycler® 384 (or 96) Real-Time PCR system (Roche). All reactions were carried out in more than three independent technical replicates for each biological sample. The data were analyzed using the $2^{-\Delta\Delta CT}$ calculation method. The primer sequences used for qRT-PCR are listed in Table S3.

Immunohistochemistry

Tissue processing and immunostaining were carried out as described previously.[74,75] Tissue samples were fixed with 4% paraformaldehyde in PBS for 15-30 min, and gradient-dehydrated with 10% and 20% sucrose solution each for at least 15 min, and then with 30% sucrose solution at 4 °C overnight. Cryosections were cut at a thickness of 14 μm. For wholemount retinas, the dorsal pole and laterality of each eye were marked right after euthanasia and before fixation. Retinas were dissected as flattened wholemounts by making four radial cuts, an extra cut was made on the dorsal pole. Retinal sections and wholemounts were blocked in 5% normal donkey serum in PBST (0.3% Triton X-100 in PBS, pH7.3), and then incubated with primary antibodies overnight (for sections) or for 48 hrs (for wholemounts) at 4°C. After three-time washes with PBST, the samples were incubated with secondary antibodies conjugated with Alexa Fluor 488 or 594 (Life Technologies) and 4′,6-diamidino-2-phenylindole (DAPI) for 1 hr at room temperature. Images were captured by a Zeiss LSM 700 confocal microscope.

Automated Western immunoblotting

Total protein was isolated from mouse retinas using the RIPA buffer (Beyotime) and quantified using the BCA protein assay (Beyotime). The Simple Western immunoblotting was performed on a PeggySue (ProteinSimple) using the Size Separation Master Kit with Split Buffer (12–230 kDa) according to the manufacturer's standard instruction as previously described.[76] The protein extract from each sample was loaded to the Wes plate at the final concentration of 1 μg/μl and the following antibodies were used: anti-MAF1(GeneTex, GTX106776), anti-RFP (Rockland, 600-401-379) and anti-β-tubulin (Abcam, ab179513). The dilution factors were 1:20 for Maf1 and RFP and 1:100 for β-tubulin. The Compass software (ProteinSimple, version 6.1.0) was used for presentation of the Western immunoblots.

RNA *in situ* hybridization

RNA in situ hybridization was carried out as previously described.[77] A 774-bp *Maf1* DNA fragment was amplified by PCR from the mouse retinal cDNA using the following primers (from 5′ to 3′): CTCGAGATGAAGCTATTGGAGAACTC and GGATCCCATACAGATCACTGGAACCC. Subsequently, it was subcloned into the pBluescript II KS(+) vector for RNA probe preparation. Eyecups were fixed overnight in 4% paraformaldehyde in PBS at 4°C and sectioned at 14 μm. Digoxigenin-labeled *Maf1* probes were prepared following the manufacturer's protocol (Roche Diagnostics).

Optic coherence tomography (OCT) analysis

For OCT, imaging was conducted in at least 3 *Maf1*$^{-/-}$ or control one-month-old mice. Animals were anesthetized with intraperitoneal injection of chloral hydrate (4.5 μg/g body weight). Pupils were dilated by tropicamide phenylephrine eye drops, and the eyes were kept moist with a drop of hypromellose. OCT images were captured using the Spectralis OCT instrument (Heidelberg, Germany). A 30D standard ophthalmic non-contact slit lamp lens (Volk Optical Inc., USA) was positioned in front of the Heidelberg Spectralis optic. Volume scans centered on the optic nerve head were acquired in the automatic real-time mode (ART), averaging 100 frames per image. Retinal thickness was measured from the GCL to the edge of ONL.

Hematoxylin-eosin (HE) staining and thickness measurement

Eyeballs were fixed overnight in FAS Eyeball Fixator (Servicebio) and paraffin-embedded. Tissue blocks were sectioned at 15 μm followed by HE staining. Retinal thickness was measured from the GCL to the edge of the ONL using the ImageJ software.

Lens organ culture

One-month-old control and *Maf1*$^{-/-}$ mice were sacrificed by CO_2 inhalation. The eyeballs were removed and the lenses were carefully dissected by a posterior approach.[78] Dissected lenses were placed in a well of a 24-well culture plate containing 1.5 ml medium199 (Sigma), then incubated at 37°C with a 5% CO_2 gas phase for 24 hrs or 48 hrs.

Electroretinography (ERG)

Electroretinograms were recorded from two-month-old or six-month-old *Maf1*$^{-/-}$ mice and age-matched control animals using the amplifier of the RETI-scan system (Roland Consult, Germany) at a sampling rate of 2 kHz as described previously.[79] All animals were recorded under the same settings and conditions. After overnight dark adaption, mice were anesthetized with intraperitoneal injection of chloral hydrate (4.5 μg/g body weight). Pupils were dilated with tropicamide phenylephrine eye drops. Scotopic recordings were obtained from dark-adapted mice at increasing light intensities ranging from 0.0003 to 10 cd.s/m^2. Thereafter, photopic recordings were performed following a 5-min light adaptation. Several levels of light stimuli ranging from 0.3 to 30 cd.s/m^2 were used for photopic recordings. For each condition (scotopic and photopic), 6 responses were averaged for each luminance of flash stimuli. The stimulation interval ranged from 2-10 s at low intensities and 1 min at intensities greater than 3.0 cd s/m^2.

RNA-SEQ AND SCRNA-SEQ ANALYSES

RNA-seq analysis was carried out as described.[71,80] In brief, for RNA-seq experiment at each developmental stage (P0 and P8), three *Maf1*$^{-/-}$ mice and three control mice were used, and the retinas from each animal were collected as one RNA-seq sample. Total RNA was isolated from P0 or P8 wild-type and *Maf1*$^{-/-}$ retinas for library preparation. Ribosomal RNA was depleted prior to RNA-seq library preparation. The obtained sequence reads were trimmed and mapped to the mm10 mouse reference genome.

For single-cell RNA sequencing (scRNA-seq) analysis, retinas were collected from P3 and P7 *Maf1*$^{-/-}$ and control mice. Single-cell library construction, sequencing, Cell Ranger processing, and Seurat analysis were performed as described.[43,71] In brief, after removal of cell doublets with Scrublet,[70] most of the Seurat analyses were carried out using default parameters. When merging WT and *Maf1*$^{-/-}$ cells, we used the ScaleData function to regress out various sources of heterogeneity including batch effects and cell cycle scores with the following parameters: vars.to.regress = c("genotype", "S.Score", "G2M.Score", "percent.mt", "nCount_RNA", "nFeature_RNA"). Unsupervised cell clusters were identified using the FindClusters function with default parameters. Then the clusters of microglia, astrocytes and endothelial cells were removed by the expression of *C1qc* and *Ccl3, Gfap* and *S100b, and Tek*, respectively. To make biologically meaningful comparative analyses of the P3 and P7 WT and *Maf1*$^{-/-}$ retinal cells, we refined the cell clusters by merging some smaller clusters based on the expression of lineage marker genes and known cell lineage trajectories during mouse retinal development[42] (Figures S9A and S9B). For instance, at P7, all unsupervised clusters expressing high levels of *Sox2* were merged into the C1 cluster (nRPCs) (Figure S9B). Similarly, C2 cells (tRPCs) express high levels of *Otx2* but not *Isl1* or *Nrl*; the bipolar cell lineage clusters C3 and C4 express *Isl1* and *Bhlhe23*, the cone cluster C8 expresses *Opn1sw*, and the amacrine cell cluster C9 expresses *Tfap2a/2b* (Figure S9B).

The pseudotime trajectory analysis was conducted using Monocle 3 with default parameters,[72] and clusterProfiler was applied to perform the GO (pvalueCutoff = 0.01, qvalueCutoff = 0.05) and KEGG (pvalueCutoff = 0.05, qvalueCutoff = 0.05) pathway enrichment analyses.[81]

In vitro retinal explant culture

Retinal explant culture was conducted as previously described.[82] In brief, the eyeballs were isolated from P0 *Maf1*$^{-/-}$ and control mice, from which retinal cups were made by carefully removing the sclera, choroid and lens. Four incisions were made from the margin of the retinal cup half way through toward the bottom at the 0, 3, 6, and 9 o'clock positions. Three to four retinas were transferred using a pipette onto a Millipore Millicell Cell Culture Insert which was then placed into a 6-well plate with 1 ml culture medium [DMEM/F12-Glutamax (Gibco), 10% ES-fetal bovine serum (Gibco), 1% penicillin/streptomycin (Gibco), 1% N2 (Gibco), 0.5 μM retinoic acid (Sigma), 0.1 mM taurine (Sigma)] in each well. The plate was subsequently transferred into a cell culture incubator (37°C, 5% CO_2). For treatment with the RNA Pol III inhibitor, 10 or 20 μM ML-60218 (MCE) was added to the culture medium.

CUT&Tag assay

CUT&Tag was performed as described previously[83] using the CUT&Tag-IT™ Assay Kit (Active Motif) according to the manufacturer's instructions. For each experiment, 2 x 10^5 retinal cells isolated from P7 C57BL/6 mice were used. PCR was performed to amplify the libraries after DNA extraction. To analyze the CUT&Tag data, sequence reads were aligned to the mm10 mouse reference genome by HISAT2.[73] The HOMER (Hypergeometric Optimization of Motif EnRichment, http://homer.ucsd.edu/homer/index.html) software suite was used to perform peak calling, determine peak position and distribution, and identify binding motifs and peak-associated genes as described previously.[80,84] GO and KEGG pathway enrichment analyses of peak-associated genes were carried out using clusterProfiler.[81]

Dual-luciferase reporter assays

DNA fragments containing Maf1 binding sites identified by CUT&Tag analysis or Maf1 mutant binding sites (Table S4) were subcloned into the pGL3-promoter and/or pGL3-basic reporter vectors (Promega), and that containing the *Maf1* open reading frame was inserted into the pCI expression vector (YouBio). Dual-luciferase reporter assay was carried out as described.[85] In brief, reporter and expression plasmids were co-transfected into 293T cells together with the control Renilla luciferase reporter vector pRL-TK (Promega). Following transfection and incubation, luciferase activities were measured using a dual-luciferase reporter assay system (Beyotime) and the Infinite M200 Pro Nanoq microplate reader (TECAN). All assays were independently repeated at least three times.

EdU, BrdU and TUNEL labeling

EdU and TUNEL labeling was performed as previously described.[74,86] EdU labeling was carried out using the Click-iT™ EdU Cell Proliferation Kit (Thermo Fishers). Timed pregnant mice or age-specific mice were injected with EdU solution and sacrificed 2 hrs later. Embryos or eyeballs were collected, fixed, and processed according to standard immunostaining protocol. EdU staining was performed according to the procedure provided by the kit. TUNEL assay was performed using the *In Situ* Cell Death Detection Kit (Roche Diagnostics) following the manufacturer's protocol. Retinal sections were prepared as described above, and the number of $TUNEL^+$ apoptotic cells was counted.

For EdU and BrdU dual labeling, solutions of BrdU and EdU were dissolved in dimethyl sulfoxide (DMSO) and protected from light. Pregnant mice were weighed, and intraperitoneally injected with 25 mg/kg EdU solution. One and half hours later, an intraperitoneal injection of the BrdU solution (50 mg/kg) was given. Half an hour after the second injection, the animals were euthanized and the embryonic retinas were collected and processed as described above. The combined immunostaining for BrdU and Ki67 and EdU visualization were carried out as described.[87] In brief, antigen retrieval was performed prior to incubation with the BrdU and Ki67 antibodies using the BrdU Kit for IHC/ICC Immunofluorescence (Thermo Fishers). Then EdU labeling was carried out using the Click-iT™ EdU Cell Proliferation Kit (Thermo Fishers). The samples were then incubated for a minimum of 2 hours at room temperature or overnight at 4°C with BrdU and Ki67 antibodies. Finally, the samples were incubated with secondary antibodies conjugated with Alexa Fluor 488 or 647 (Life Technologies) and 4′,6-diamidino-2-phenylindole (DAPI) for 1 hr at room temperature. The calculation formulae for the total cell cycle length (Tc) and S-phase length (Ts) were described previously[45–47]: $Ts = injection\ interval \times \frac{BrdU^+\ cells}{EdU^+\ only\ cells}$ and $c = injection\ interval \times \frac{Ki67^+\ cells}{EdU^+\ only\ cells}$.

QUANTIFICATION AND STATISTICAL ANALYSIS

At least three retinas were analyzed each for control and *Maf1*$^{-/-}$ animals. Each data point of cell quantification in sections or retinal whole-mounts was averaged from 6-8 non-overlapping optical fields in similar retinal regions. To score sufficient number of cells for statistical analysis, each optical field was photographed using the confocal microscope at 200x (a square of 320 μm x 320 μm) or 400x (a square of 160 μm x 160 μm) magnification depending on the density of labeled cells. For cell quantification in retinal sections, the optical field was photographed from the central region of the retina, parallel to the tangent line of the retinal region, and should include all the labeled cells in all retinal layers. Statistical analysis was performed using the GraphPad Prism 8.0 and Microsoft Excel computer programs. The results are expressed as mean ± SEM for experiments conducted at least in triplicates. Unpaired two-tailed Student's t test was used to assess the differences between two groups. For all ERG data, two-way ANOVA with the Holm-Sidak correction was used to test for significance. A value of $p < 0.05$ was considered statistically significant.